Study of b-hadron decays to $\Lambda_c^+ h^- h'^-$ final states

The LHCb collaboration

E-mail: bhagyashree.pagare@cern.ch

ABSTRACT: Decays of Ξ_b^- and Ω_b^- baryons to $\Lambda_c^+ h^- h'^-$ final states, with $h^- h'^-$ being $\pi^- \pi^-$, $K^- \pi^-$ and $K^- K^-$ meson pairs, are searched for using data collected with the LHCb detector. The data sample studied corresponds to an integrated luminosity of $8.7\,\text{fb}^{-1}$ of pp collisions collected at centre-of-mass energies $\sqrt{s} = 7$, 8 and 13 TeV. The products of the relative branching fractions and fragmentation fractions for each signal mode, relative to the $B^- \to \Lambda_c^+ \overline{p} \pi^-$ mode, are measured, with $\Xi_b^- \to \Lambda_c^+ K^- \pi^-$, $\Xi_b^- \to \Lambda_c^+ K^- K^-$ and $\Omega_b^- \to \Lambda_c^+ K^- K^-$ decays being observed at over $5\,\sigma$ significance. The $\Xi_b^- \to \Lambda_c^+ K^- \pi^-$ mode is also used to measure the Ξ_b^- production asymmetry, which is found to be consistent with zero. In addition, the $B^- \to \Lambda_c^+ \overline{p} K^-$ decay is observed for the first time, and its branching fraction is measured relative to that of the $B^- \to \Lambda_c^+ \overline{p} \pi^-$ mode.

KEYWORDS: B Physics, Branching fraction, Hadron-Hadron Scattering, Heavy Quark Production

Contents

1 Introduction

The large production rate of b hadrons in LHC collisions has enabled a vastly increased range of b-baryon decays to be studied. The majority of measurements in this sector have so far been made with Λ_b^0 baryons, with only relatively few Ξ_b^- and Ω_b^- decays observed [1–9]. New and improved measurements of the production and decays of b baryons will constrain QCD models and also reduce systematic uncertainties in future measurements of the properties of related decays. In particular, knowledge of production asymmetries is necessary to make precise searches for *CP* violation in b-baryon decays [4]. Existing measurements of the production rates and asymmetries of Ξ_b^- baryons, obtained using the $\Xi_b^- \to J/\psi \Xi^-$ decay [10], have large uncertainties so improvements are well motivated. Additionally, the phase-space distribution of multibody b-baryon decays can be probed to investigate the spectroscopy of charm baryons, including studies of potentially exotic hadrons.

At present there are no results on Ξ_b^- and Ω_b^- decays to $\Lambda_c^+ h^- h'^-$ final states, where h and h' are K or π mesons. Figure 1 shows possible decay diagrams for three such processes, specifically those where the branching fractions are expected to be largest. The $\Xi_b^- \to \Lambda_c^+ K^- \pi^-$ decay shown in figure 1 (left) and the $\Omega_b^- \to \Lambda_c^+ K^- K^-$ mode shown in figure 1 (right) are Cabibbo-favoured processes, while the $\Xi_b^- \to \Lambda_c^+ K^- K^-$ decay shown in figure 1 (centre) is Cabibbo-suppressed. No tree-level diagram exists for the $\Xi_b^- \to \Lambda_c^+ \pi^- \pi^-$, $\Omega_b^- \to \Lambda_c^+ K^- \pi^-$ and $\Omega_b^- \to \Lambda_c^+ \pi^- \pi^-$ decays, so these are expected to be significantly suppressed.

In this paper, a search for Ξ_b^- and Ω_b^- decays to the $\Lambda_c^+ h^- h'^-$ final states is described. The analysis is based on the full Run 1 (3 fb^{-1} of pp collisions at $\sqrt{s} = 7$ and 8 TeV) and Run 2 (5.7 fb^{-1} at $\sqrt{s} = 13$ TeV) data sample collected with the LHCb detector. The $B^- \to \Lambda_c^+ \bar{p} \pi^-$ decay, which has been previously observed [11, 12], is used as a control and
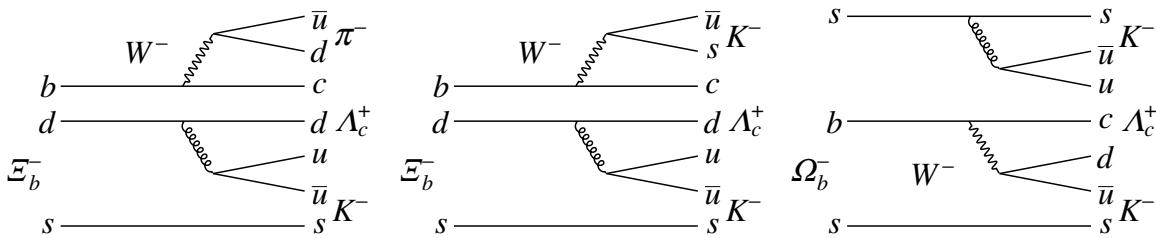
**Figure 1.** Examples of decay diagrams for the (left) $\Xi_b^- \to \Lambda_c^+ K^- \pi^-$, (centre) $\Xi_b^- \to \Lambda_c^+ K^- K^-$ and (right) $\Omega_b^- \to \Lambda_c^+ K^- K^-$ channels.

normalisation channel. The previously unobserved $B^- \to \Lambda_c^+ \overline{p} K^-$ decay is also studied as part of the analysis. In all cases, the Λ_c^+ baryon is reconstructed in the $pK^-\pi^+$ final state. The inclusion of charge-conjugate processes is implied throughout, except where asymmetries are discussed. The analysis is performed blind, such that the signal mass regions for both the Ξ_b^- (5735–5865 MeV/c^2) and Ω_b^- (5977–6107 MeV/c^2) baryons are not inspected until analysis procedures are established; the B^- modes, however, are not blinded during the analysis.

Ratios of fragmentation fractions times branching fractions of two channels are determined from ratios of efficiency-corrected yields. In the case that decays of the same b hadron, X_b, to final states generically labelled Y and Z are considered, the ratio of branching fractions is determined as

$$\frac{\mathcal{B}(X_b \to Y)}{\mathcal{B}(X_b \to Z)} = \frac{N(Y)/\langle \epsilon(Y) \rangle}{N(Z)/\langle \epsilon(Z) \rangle} = \frac{\sum_{i=0}^{n_Y} w_i^Y/\epsilon_i^Y}{\sum_{i=0}^{n_Z} w_i^Z/\epsilon_i^Z} = \frac{N^{\mathrm{corr}}(Y)}{N^{\mathrm{corr}}(Z)} \,. \tag{1.1}$$

The yield obtained from the fit to the X_b-candidate mass distribution, N, is equal to $\sum_{i=0}^{n} w_i$ where w_i are signal weights [13] obtained from the same fit for all the n candidates in the fit. Variation of the efficiency across the phase space of the decay is taken into account by use of candidate-by-candidate efficiencies, ϵ_i, which depend on position in the decay phase-space and year of data taking. The efficiencies are determined from simulation with corrections, discussed below, applied in order to describe data more accurately. The efficiency-corrected yield is then $N^{\mathrm{corr}} = \sum_{i=0}^{n} w_i/\epsilon_i$, and an effective average efficiency can be defined as $\langle \epsilon \rangle = N/N^{\mathrm{corr}}$. In case the yield of a particular channel is not significant, the candidate-by-candidate efficiency correction of eq. (1.1) will not be reliable, and an average efficiency obtained directly from simulation with an assumption on the phase-space distribution is used instead. In this case, the effect of the unknown phase-space distribution will be a source of systematic uncertainty.

When decays of different b hadrons are considered, eq. (1.1) is modified so that the left-hand side is multiplied by the appropriate ratio of fragmentation fractions, but the procedure is otherwise identical. The fragmentation fractions quantify the probability that a b quark produced in the pp collision hadronises into a particular b hadron. The fragmentation fractions can depend on pp collision centre-of-mass energy, and therefore all ratios are determined separately for Run 1 and Run 2. Combined results are obtained where appropriate, taking correlations of systematic uncertainties into account.

For a channel $X_b \to Y$ with sufficient yield, the charge-conjugate processes can be separated to determine the X_b production asymmetry, $\mathcal{A}_{\mathrm{prod}}$, from the measured efficiency-

corrected yield asymmetry,

$$\mathcal{A}_{\text{meas}}\left(X_b \to Y\right) = \frac{\sum_{i=0}^{n_Y} \frac{w_i}{\epsilon_i} - \sum_{i=0}^{n_{\bar{Y}}} \frac{w_i}{\bar{\epsilon}_i}}{\sum_{i=0}^{n_Y} \frac{w_i}{\epsilon_i} + \sum_{i=0}^{n_{\bar{Y}}} \frac{w_i}{\bar{\epsilon}_i}} = \frac{N^{\text{corr}}(X_b \to Y) - N^{\text{corr}}(\bar{X}_b \to \bar{Y})}{N^{\text{corr}}(X_b \to Y) + N^{\text{corr}}(\bar{X}_b \to \bar{Y})}, \quad (1.2)$$
$$= \mathcal{A}_{CP}\left(X_b \to Y\right) + \mathcal{A}_{\text{prod}}\left(X_b\right).$$

Here, the weights w_i in all sums are obtained from a single fit to the sample including both charge conjugate final states, but sums over different candidates are performed for the two states. The sense of the asymmetry is defined as being between the X_b hadron that contains a b quark and its $\bar{X}_b$ antiparticle that contains a $\bar{b}$ quark. The efficiency maps used to obtain the N^{corr} values also differ for the two charge conjugate final states, and are denoted as ϵ and $\bar{\epsilon}$. The use of separate efficiency maps corrects for detection asymmetry, although potential mismodelling of ϵ and $\bar{\epsilon}$ must be accounted for as a source of systematic uncertainty. For decays where no CP violation is expected, i.e. where $\mathcal{A}_{CP} = 0$ can be assumed, one has $\mathcal{A}_{\text{meas}} = \mathcal{A}_{\text{prod}}$. This is the case for the channels studied here, which are expected to be dominated by tree-level diagrams as shown in figure 1.

Production asymmetries, and the relative fragmentation fractions of different hadrons, can depend on kinematics. The above approach can be extended to study such effects, by making measurements in bins of, for example, b-hadron transverse momentum. In this case the sum in eq. (1.2) includes only events in the relevant bin, and the efficiency maps are those appropriate for that bin.

2 Detector and simulation

The LHCb detector [14, 15] is a single-arm forward spectrometer covering the pseudorapidity range $2 < \eta < 5$, designed for the study of particles containing b or c quarks. The detector includes a high-precision tracking system consisting of a silicon-strip vertex detector surrounding the pp interaction region [16], a large-area silicon-strip detector located upstream of a dipole magnet with a bending power of about $4\,\text{T}\,\text{m}$, and three stations of silicon-strip detectors and straw drift tubes [17, 18] placed downstream of the magnet. The tracking system provides a measurement of the momentum, p, of charged particles with relative uncertainty that varies from 0.5% at low momentum to 1.0% at $200\,\text{GeV}/c$. The minimum distance of a track to a primary pp collision vertex (PV), the impact parameter (IP), is measured with a resolution of $(15 + 29/p_\text{T})\,\mu\text{m}$, where p_T is the component of the momentum transverse to the beam, in GeV/c. Different types of charged hadrons are distinguished using information from two ring-imaging Cherenkov detectors [19]. Photons, electrons and hadrons are identified by a calorimeter system consisting of scintillating-pad and preshower detectors, an electromagnetic and a hadronic calorimeter. Muons are identified by a system composed of alternating layers of iron and multiwire proportional chambers [20].

The online event selection is performed by a trigger [21, 22], which consists of a hardware stage, based on information from the calorimeter and muon systems, followed by a software stage, which applies a full event reconstruction. At the hardware trigger stage, events are required to have a muon with high p_T or a hadron, photon or electron with high transverse energy in the calorimeters. For hadrons, the transverse energy threshold is $3.5\,\text{GeV}$. The

software trigger requires a two-, three- or four-track secondary vertex with a significant displacement from any primary pp interaction vertex. At least one charged particle must have a transverse momentum $p_T > 1.6\,\text{GeV}/c$ and be inconsistent with originating from a PV. A multivariate algorithm [23, 24] is used for the identification of secondary vertices consistent with the decay of a b hadron. In the offline selection, trigger signals are associated with reconstructed particles. Selection requirements can therefore be made on the trigger selection itself and on whether the decision was due to the signal candidate, other particles produced in the pp collision, or a combination of both.

Simulation is used to model the effects of the detector acceptance and the imposed selection requirements, as well as to study potential backgrounds. In the simulation, pp collisions are generated using PYTHIA [25, 26] with a specific LHCb configuration [27]. The signal processes are generated with the FLATSQDALITZ model, which generates events uniformly in the square Dalitz plot as described in ref. [41]. Decays of unstable particles are described by EVTGEN [28], in which final-state radiation is generated using PHOTOS [29]. The interaction of the generated particles with the detector, and its response, are implemented using the GEANT4 toolkit [30, 31] as described in ref. [32]. The underlying pp interaction is reused multiple times, with an independently generated signal decay for each [33]. The response of the ring-imaging Cherenkov detectors in simulation is known to not match the response in data, so the corresponding particle identification (PID) variables in the simulation samples are corrected based on calibration data samples of $D^{*+} \to D^0\pi^+$, $D^0 \to K^-\pi^+$ decays for kaons and pions, and $\Lambda_c^+ \to pK^-\pi^+$ decays for protons [34]. The correction technique transforms the variables such that they match the data distributions, accounting for dependence on track kinematics and event multiplicity, while retaining correlations between different PID variables.

3 Selection

Candidate signal and control channel decays are formed from five final-state tracks, where three of the tracks are consistent with originating from the Λ_c^+ decay and the other two are consistent with originating from the b-hadron decay. The Λ_c^+ candidates are required to have reconstructed mass in the range $2260 < m(pK^-\pi^+) < 2310\,\text{MeV}/c^2$. The hardware trigger decision is required to have been caused by either calorimeter clusters associated with one or more of the final-state particles, or by particles produced in the pp bunch crossing not involved in forming the X_b candidate. Candidates with clone tracks, reconstructed from the same detector hits, are removed. The candidate is associated with the PV in the pp bunch crossing with which it forms the smallest value of χ_{IP}^2, defined as the difference in χ^2 of a given PV reconstructed with and without the considered particle. Candidates are selected with an initial filtering, to reduce the sample size to a manageable level while maintaining high efficiency, followed by the use of multivariate algorithms to reject background processes in an optimal way. Two dedicated boosted decision tree (BDT) algorithms, trained using the XGBoost method [35] separately for the Run 1 and Run 2 samples, are used to separate signal from combinatorial background. Particle identification variables are used to suppress backgrounds involving misidentified final-state particles, including cross-feed between the different signal final states. The same BDT requirements are used to select $\Xi_b^- \to \Lambda_c^+ h^- h'^-$, $\Omega_b^- \to \Lambda_c^+ h^- h'^-$ and $B^- \to \Lambda_c^+ \bar{p}h^-$ decays; only PID requirements distinguish the different final states.

The first BDT algorithm is designed to distinguish true $\Lambda_c^+ \to pK^-\pi^+$ decays originating from b-hadron decays from random combinations of tracks that produce fake Λ_c^+ candidates. It uses as inputs the Λ_c^+ candidate's χ_{IP}^2, together with the significance of the separation from the Λ_c^+ decay vertex of each of the PV and the X_b decay vertex, and the angle between the Λ_c^+-candidate momentum vector and the vector from the PV to the Λ_c^+ decay vertex. Variables that characterise the goodness of fit of each of the three tracks and their assumed common vertex are also included, together with the highest p_{T} of the three tracks and PID variables for each of them. This BDT classifier is trained with a signal sample of the three Ξ_b^- decays combined taken from simulation and a background sample taken from sideband regions of the Λ_c^+-candidate mass distribution in data, defined as $2190 < m(pK^-\pi^+) < 2241\,\mathrm{MeV}/c^2$ and $2331 < m(pK^-\pi^+) < 2380\,\mathrm{MeV}/c^2$. A loose requirement is applied on the first BDT output to remove a significant fraction of the fake Λ_c^+ backgrounds.

The second BDT classifier suppresses combinatorial background composed of a true Λ_c^+ hadron with two random tracks. The input variables are the X_b-candidate's χ_{IP}^2 and p_{T}, together with the significance of the separation between the X_b decay vertex and the PV and the χ^2 of the X_b vertex. The highest p_{T} among the X_b decay products and the sum of their χ_{IP}^2 values are also used, together with a variable that characterises the isolation of the candidate relative to other particles produced in the pp collision in terms of a p_{T} asymmetry [36]. Finally, the first BDT output is taken as an input to the second. This second BDT classifier is trained using a signal sample taken from simulation and a background sample taken from sideband regions of the X_b-candidate mass distribution in data, defined as $5400 < m(X_b) < 5742\,\mathrm{MeV}/c^2$ and $5852 < m(X_b) < 7500\,\mathrm{MeV}/c^2$.

The PID variables for Λ_c^+ decay products are included in the first BDT algorithm, and are not used further in the selection. For the tracks originating directly from the X_b decay, kaon and pion candidates are distinguished with requirements in the two-dimensional plane of the PID variables that characterise how well they fit each of those particle hypotheses. These requirements are optimised as described below, and are required to be mutually exclusive so that no candidate can appear in more than one final state. To select antiprotons in the $B^- \to \Lambda_c^+ \bar{p} h^-$ decays, a requirement on the consistency with the proton hypothesis is imposed. In order to ensure that reasonable PID information is available, fiducial requirements are imposed on the kinematics of all final-state tracks: $2.5 < p_{K,\pi} < 100\,\mathrm{GeV}/c$, $9.5 < p_p < 100\,\mathrm{GeV}/c$ and $2 < \eta_{p,K,\pi} < 5$. In addition, all tracks are required to be inconsistent with being muons, based on information from the muon system.

The requirement on the second BDT output is optimised using the following figure of merit (FOM) [37],

$$\mathrm{FOM}_{\mathrm{BDT}} = \frac{\epsilon_{\mathrm{sig}}}{\left(\frac{5}{2} + \sqrt{B}\right)}\,, \tag{3.1}$$

where B is the expected number of combinatorial background events in the signal region $(5770 < m(X_b) < 5830\,\mathrm{MeV}/c^2)$, obtained by extrapolating yields in data in the upper mass sideband $(5830 < m(X_b) < 6800\,\mathrm{MeV}/c^2)$, and ϵ_{sig} is the signal efficiency determined from simulation. The requirements on the kaon and pion identification variables are optimised using

$$\mathrm{FOM}_{\mathrm{PID}} = \frac{\epsilon_{\mathrm{sig}}}{\epsilon_{\mathrm{sig}} + \sum_i r_i \epsilon_{\mathrm{misID}\,i}}\,, \tag{3.2}$$

where $\epsilon_{\mathrm{misID}\,i}$ is the misidentification rate for each potential cross-feed background i, taken from simulation with PID corrections applied, and $r_i = \mathcal{B}(\mathrm{misID}\,i)/\mathcal{B}(\mathrm{sig})$ is an estimate of the branching fraction of the cross-feed background, $\mathcal{B}(\mathrm{misID}\,i)$, relative to that of the signal mode, $\mathcal{B}(\mathrm{sig})$. The optimisation of the requirements on the second BDT output and the PID variables is iterated to obtain the best overall performance. The optimised requirements on the second BDT output reject around 99% of background while retaining 40–50% of signal depending on the final state and data-taking period.

The $\Lambda_c^+ K^- \pi^-$ and $\Lambda_c^+ \overline{p} K^-$ samples contain misreconstructed candidates where the K^- from the Λ_c^+ decay is swapped with that directly from the X_b decay. These are vetoed by removing candidates that satisfy $2260 < m(p_{\Lambda_c^+} K^- \pi_{\Lambda_c^+}^+) < 2310\,\mathrm{MeV}/c^2$, where the subscript Λ_c^+ indicates that the particle is one of the Λ_c^+ decay products while the absence of a subscript indicates that the particle originates directly from the X_b decay. Backgrounds also occur due to $\Lambda_b^0 \to \Lambda_c^+ \pi^-$ or $\Lambda_b^0 \to \Lambda_c^+ K^-$ decays combined with an extra track. This source includes true $\Xi_b^- \to \Lambda_b^0 \pi^-$ decays [8], which are considered a background to this analysis, as well as cases where the extra track does not originate from the same b-hadron decay. Vetoes that remove candidates with $5500 < m(\Lambda_c^+ \pi^-) < 5700\,\mathrm{MeV}/c^2$ and $5500 < m(\Lambda_c^+ K^-) < 5700\,\mathrm{MeV}/c^2$ are applied in the relevant final states to remove these backgrounds. The loss in signal efficiency due to these veto requirements is considered as a source of systematic uncertainty.

Potential backgrounds from X_b decays to the same final-state particles without intermediate Λ_c^+ baryons are investigated by inspecting the X_b-candidate mass distribution for candidates with Λ_c^+-candidate masses both below and above the region populated by signal. No significant contribution is visible and therefore no additional selection requirements are imposed to remove such backgrounds.

Backgrounds are expected from b-hadron decays to final states of $\Lambda_c^+ h^- h'^-$ plus one or more low-momentum particles, subsequently referred to as partially reconstructed backgrounds. These include b-hadron decays to $\Sigma_c^{+(++)} h^- h'^-$ final states with $\Sigma_c^{+(++)} \to \Lambda_c^+ \pi^{0(+)}$. Similar arguments hold for partially reconstructed backgrounds to the $B^- \to \Lambda_c^+ \overline{p} h^-$ channels. Due to the missing particles, these backgrounds tend to peak at X_b-candidate mass values below the signal peaks. In order to minimise dependence on precise modelling of these backgrounds, the mass ranges retained for the fits are $5550 < m(X_b) < 6800\,\mathrm{MeV}/c^2$ for the signal channels and $5200 < m(X_b) < 6000\,\mathrm{MeV}/c^2$ for the B^- channels.

A small fraction ($< 1\%$) of selected events contain more than one candidate. All are retained, and the presence of multiple candidates is considered as source of systematic uncertainty.

4 Determination of signal yields

Fits to the X_b-candidate mass distributions are performed to determine the yields of the channels under study. Simultaneous unbinned extended maximum-likelihood fits are implemented to allow parameters to be shared between the samples. One simultaneous fit is performed for the three signal final states, and another for the two B^- modes, with separate fits for the Run 1 and Run 2 samples. The fits include components to describe the signals, and contributions due to cross-feed, partially reconstructed decays and combinatorial background.

The signal components are described using the sum of two Crystal Ball (CB) functions [38], with a common central value and width, and independent tails to each side of the peak. The tail parameters and the relative fraction of the two CB functions are determined from fits to simulation samples and are fixed in the fit to data.

Cross-feed between the signal modes occurs due to misidentification of one of the particles originating directly from the X_b decay. The X_b-candidate mass distributions of these backgrounds depend on the momentum and misidentification probability of that particle. Therefore, these shapes depend (albeit fairly weakly) on the phase-space distribution of the misidentified decay. For the $B^- \to \Lambda_c^+ \bar{p} \pi^-$ channel there are previous investigations of its resonant structure [11, 12]; however these were made with samples much smaller than available in this study. Since the analysis of the B^- modes is not blind, the phase-space distributions observed in data are used to weight the simulation and obtain a best estimate of the shape of the cross-feed background components. On the other hand, since the analysis is performed blind for the Ξ_b^- and Ω_b^- baryon decays, their phase-space distributions are taken from simulation without any phase-space weighting. This procedure is considered as a source of systematic uncertainty. The distribution for each sample under each $K \leftrightarrow \pi$ misidentification hypothesis is fitted with a double CB function. Misidentification of protons as pions or kaons, and vice versa, does not lead to background contributions in the fitted mass ranges.

Residual partially reconstructed backgrounds due to the decays $\Xi_b^- \to \Sigma_c^+ h^- h'^-$ and $\Xi_b^0 \to \Sigma_c^{++} h^- h'^-$ are described as a single component in the fit. The shape is investigated with a simplified simulation [39], and is modelled with a superposition of Gaussian kernels [40]. Partially reconstructed backgrounds to the B^- modes are found to be negligible in the chosen mass fit range. The combinatorial background is modelled with an exponential shape. The slope of the exponent in each final state is a free parameter in the fit.

The yields of all signal, partially reconstructed, and combinatorial components are free parameters in the simultaneous fit to the three signal final states. The yields of cross-feed backgrounds are constrained relative to the signal yield of the same decay when it is correctly reconstructed, based on knowledge of the relative misidentification rates and correct identification efficiencies. The shapes of all components are fixed, except that the slope parameters of the exponential function used to describe combinatorial background in each final state are free to vary independently of each other. In addition, a peak position offset and a width scale factor, which account for possible discrepancies between data and simulation and that are shared between all components described by a double CB function, are free parameters of the fit. In total there are seventeen free parameters in each simultaneous fit to the signal final states: six signal yields, three combinatorial background yields and three slope parameters, three partially reconstructed background yields, and the peak shift and width scale parameters. There are, in addition, ten Gaussian constraints that control the yields of the cross-feed backgrounds.

A similar configuration is used for the simultaneous fit to the two B^- modes. In this case there are eight free parameters: two signal yields, two combinatorial background yields and two slope parameters, as well as the peak shift and width scale parameters. In addition, there are two Gaussian constraints that control the yields of the cross-feed backgrounds.

	Run 1	Run 2
$N(\Xi_b^- \to \Lambda_c^+ K^- K^-)$	9.1 ± 3.6	19.4 ± 5.2
$N(\Xi_b^- \to \Lambda_c^+ K^- \pi^-)$	137 ± 14	471 ± 24
$N(\Xi_b^- \to \Lambda_c^+ \pi^- \pi^-)$	23 ± 11	14 ± 9
$N(\Omega_b^- \to \Lambda_c^+ K^- K^-)$	6.7 ± 2.8	22.6 ± 5.2
$N(\Omega_b^- \to \Lambda_c^+ K^- \pi^-)$	3.2 ± 3.4	4.9 ± 3.5
$N(\Omega_b^- \to \Lambda_c^+ \pi^- \pi^-)$	2.8 ± 6.5	-3.0 ± 4.2
$N(B^- \to \Lambda_c^+ \overline{p} K^-)$	66 ± 9	288 ± 18
$N(B^- \to \Lambda_c^+ \overline{p} \pi^-)$	2020 ± 50	8410 ± 90

Table 1. Fitted yields for Ξ_b^- and Ω_b^- decays to the $\Lambda_c^+ h^- h'^-$ final states, and for $B^- \to \Lambda_c^+ \overline{p} h^-$ decays.

The performance of each fit is evaluated using ensembles of pseudoexperiments. For the fit to the signal final states, this is done prior to unblinding with guessed signal yields, and subsequently repeated with the yields observed in data. For the B^- modes the yields observed in data are used in the generation of the pseudoexperiments. In all cases, the fits are found to return the signal yields with reasonable coverage and without large biases; small possible biases are accounted for as a source of systematic uncertainty.

The X_b-candidate mass distributions for the three signal final states for both Run 1 and Run 2 are shown in figures 2 and 3 with linear and logarithmic y-axis scales, respectively, with results of the fits superimposed. The mass distributions and results of the fits to the two B^- modes are similarly shown in figures 4 and 5. Pronounced peaks corresponding to $\Xi_b^- \to \Lambda_c^+ K^- \pi^-$ and $B^- \to \Lambda_c^+ \overline{p} K^-$ decays, as well as the previously established $B^- \to \Lambda_c^+ \overline{p} \pi^-$ decay, are observed. Smaller, but still clear, peaks corresponding to $\Xi_b^- \to \Lambda_c^+ K^- K^-$ and $\Omega_b^- \to \Lambda_c^+ K^- K^-$ decays are also visible. The fitted signal yields are given in table 1. The uncertainties on all fitted yields are found to be symmetric to within 20% and therefore symmetrised uncertainties are quoted in table 1; the full likelihood curves are, however, used to set upper limits on channels with yields that are not significantly different from zero, as discussed below. The significance of each of the signals is discussed in section 7.

5   Efficiency

The total efficiency includes effects from the geometrical acceptance of the LHCb detector, the reconstruction efficiency, and the probabilities to pass both trigger stages and offline selection requirements. All these effects are estimated using simulation, with data-driven corrections applied where appropriate. In particular, the efficiencies of the PID requirements can be obtained directly from the simulation samples, since the corresponding variables are corrected using calibration data.

Separate efficiency maps for each channel are obtained for each year of data taking, using square Dalitz-plot coordinates [41] to represent the phase space of the three-body decay. The use of candidate-by-candidate efficiencies, depending on position in the phase space, ensures that the distribution of decays in data is accounted for when evaluating results using
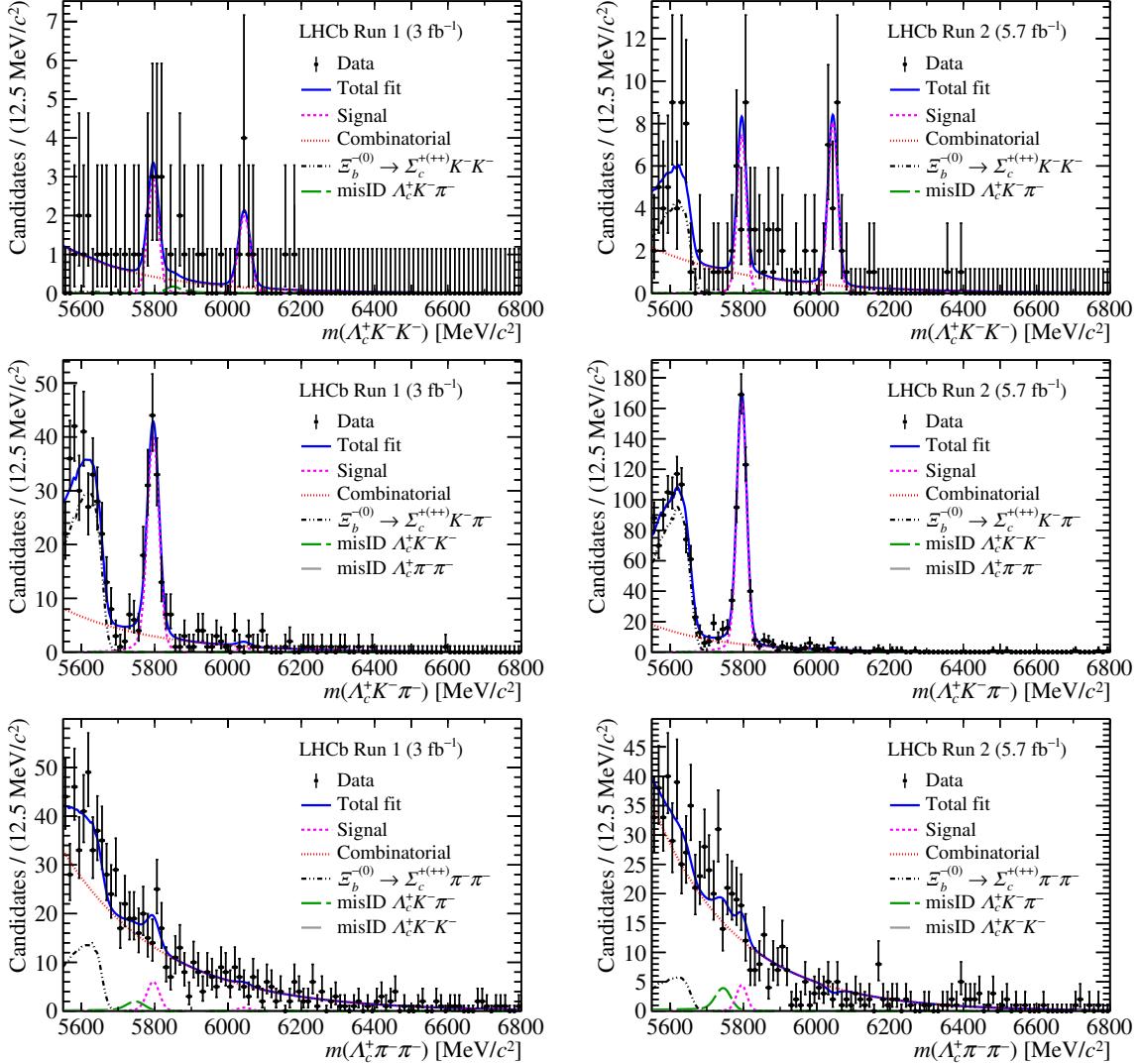
Figure 2. Mass distributions of the signal channels with results of the fit superimposed: (top) $\Lambda_c^+ K^- K^-$, (middle) $\Lambda_c^+ K^- \pi^-$ and (bottom) $\Lambda_c^+ \pi^- \pi^-$ final states for (left) Run 1 and (right) Run 2. The different components in the fit are shown as indicated in the legends, where the signal components include independent contributions from Ξ_b^- and Ω_b^- decays.

eq. (1.1). The simulated samples are additionally weighted to correct for two sources of data-simulation disagreement. The first of these is due to the Ω_b^- lifetime, where improved measurements [1, 42, 43] are available compared to the value used when generating the simulation. A weighting factor is applied to the Ω_b^- signal samples based on the difference in the decay-time distribution associated to updating the lifetime from the generated value. The second is due to the b-hadron production kinematics, which for b-baryons are not well tuned in the simulation due to the absence of previous measurements. The reconstructed $p_{\rm T}$ and pseudorapidity (η) distributions are obtained from background-subtracted data in the $B^- \to \Lambda_c^+ \overline{p} \pi^-$ and $\Xi_b^- \to \Lambda_c^+ K^- \pi^-$ channels, as shown in figures 6 and 7. The distributions obtained from $\Xi_b^- \to \Lambda_c^+ K^- \pi^-$ decays are used to weight both the Ξ_b^- and Ω_b^- signal samples.
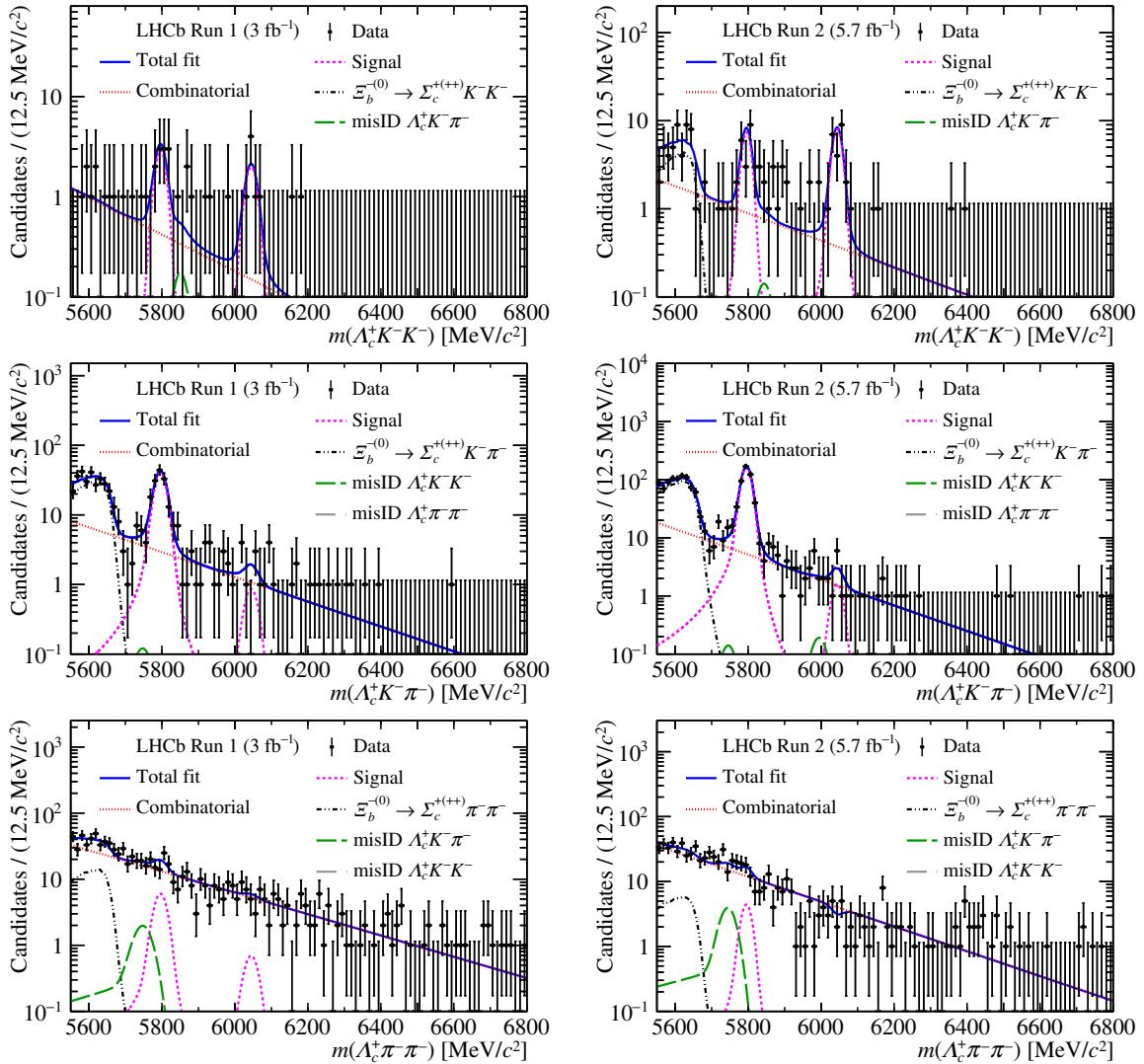
Figure 3. Mass distributions of the signal channels with results of the fit superimposed: (top) $\Lambda_c^+ K^- K^-$, (middle) $\Lambda_c^+ K^- \pi^-$ and (bottom) $\Lambda_c^+ \pi^- \pi^-$ final states for (left) Run 1 and (right) Run 2 (log scale). The different components in the fit are shown as indicated in the legends, where the signal components include independent contributions from Ξ_b^- and Ω_b^- decays.

Since the efficiencies depend quite strongly on the X_b-candidate flight distance and transverse momentum, these corrections impact the results and are a source of systematic uncertainty.

6 Systematic uncertainties

As seen in eqs. (1.1) and (1.2), each calculation of a ratio of fragmentation fractions times branching fractions or of a production asymmetry depends essentially on two inputs: the signal weights obtained from the X_b-candidate mass fits and the efficiency maps as a function of phase-space position. Sources of systematic uncertainty are hence considered as being related to one of these inputs, although in some cases the choice of which to relate to is arbitrary. Since the $B^- \to \Lambda_c^+ \overline{p} \pi^-$ control channel has the same topology as the signal
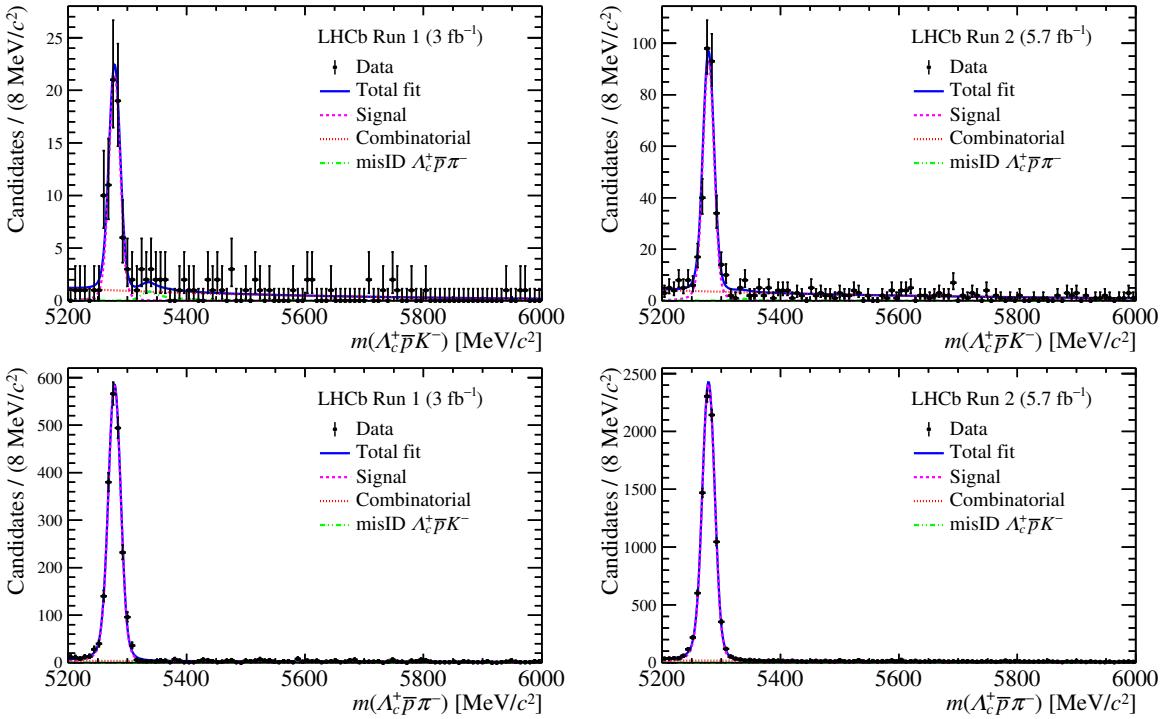
Figure 4. Mass distributions of the B^- modes with results of the fit superimposed: (top) $\Lambda_c^+ \bar{p} K^-$ and (bottom) $\Lambda_c^+ \bar{p} \pi^-$ final states for (left) Run 1 and (right) Run 2. The different components in the fit are shown as indicated in the legends.

channels, and the selection of different channels differs only by PID requirements, several potentially large systematic uncertainties are reduced in the ratios of fragmentation fractions times branching fractions.

Systematic uncertainties on the yields arise from the model chosen to fit the X_b-candidate mass distributions, from fixed parameters in the fit model, and from the dependence of the shape of the misidentified $\Xi_b^- \to \Lambda_c^+ K^- \pi^-$ component on its *a priori* unknown phase-space distribution. These uncertainties are evaluated by assessing the impact on the results of using alternative models for each of the fit components, varying fixed parameters within their uncertainties, and obtaining the misidentified $\Xi_b^- \to \Lambda_c^+ K^- \pi^-$ shape from simulation weighted to match the phase-space distribution observed in data, respectively. The alternative models considered are a combination of Johnson functions and Gaussian shapes for the signal components, second-order polynomials for the combinatorial background, shapes obtained with kernel density estimates for the cross-feed components and modified kernel density estimates for the partially reconstructed backgrounds. Systematic uncertainties due to potential biases in the fit are determined from large ensembles of pseudoexperiments generated according to the yields obtained from, and the probability density functions used in, the fit to the X_b-candidate mass distributions. Additionally, effects due to the presence of multiple candidates and from the impact of vetoing regions of the phase space are considered as being related to the yields. The former is evaluated from the impact on the results of allowing at most one candidate per pp bunch crossing, and the latter from changing the width of the veto window.
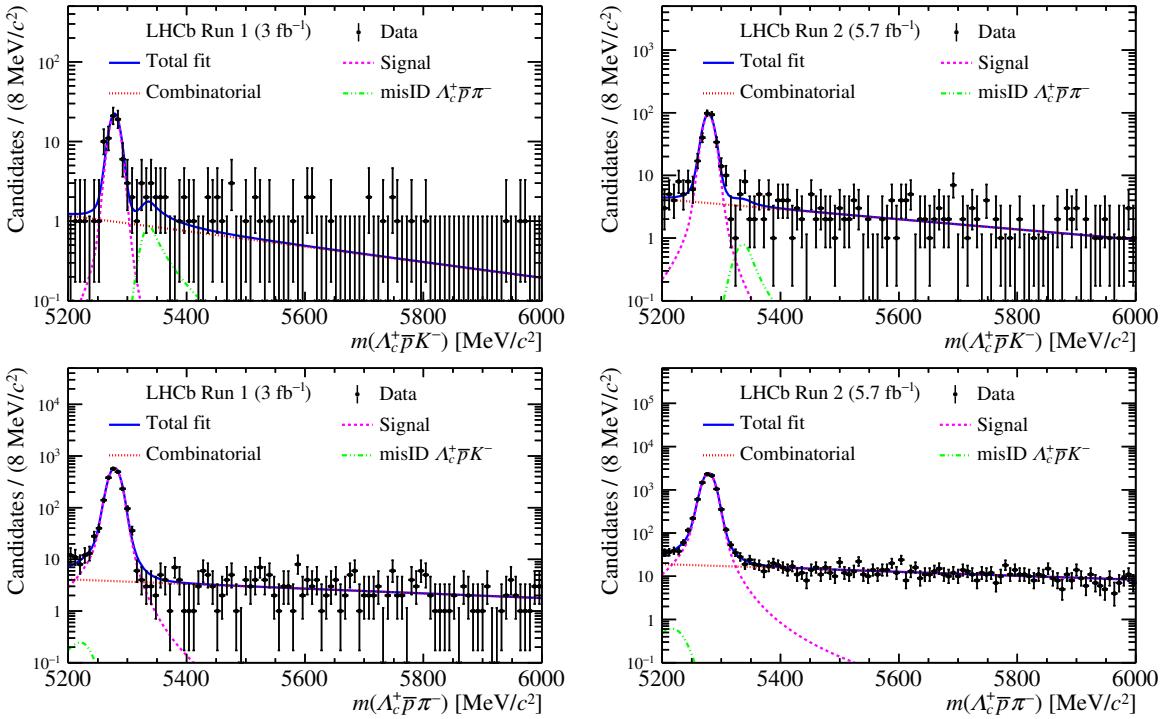
Figure 5. Mass distributions of the B^- modes with results of the fit superimposed: (top) $\Lambda_c^+\overline{p}K^-$ and (bottom) $\Lambda_c^+\overline{p}\pi^-$ final states for (left) Run 1 and (right) Run 2 (log scale). The different components in the fit are shown as indicated in the legends.

Systematic uncertainties on the efficiency maps occur due to the finite size of the simulation samples and potential inaccuracies in the simulation description of the detector and its response. The former is evaluated by varying the efficiency maps within their uncertainties, while for the latter several possible data-simulation inconsistencies are considered. These include the amount of detector material [44, 45], the efficiency of the tracking algorithms [44] and the response of the hardware trigger [46]. The impact of possible effects due to inaccuracies in the simulation description of the detector response are evaluated by weighting the simulated samples to correct the distributions of key variables. Uncertainties also arise due to the procedure to correct PID variables in simulation, and the granularity over phase space of the efficiency maps. The effect of correcting the $\Lambda_c^+ \to pK^-\pi^+$ decay model in simulation to match the latest measurement [47] is also considered as a systematic uncertainty. Uncertainty in the b-baryon production kinematics is accounted for by considering the impact on the results of changing the weighting procedure to account for only the p_{T} distribution, rather than both the p_{T} and η distributions. Finally, for channels in which the signal yield is not significant, so that the candidate-by-candidate efficiency correction procedure is not reliable, an uncertainty is assigned due to the unknown phase-space distribution.

Systematic uncertainties on the production asymmetries are evaluated in the same way as for the ratios of fragmentation fractions and branching fractions, which is possible as the measurements are made in very similar ways, as seen in eqs. (1.1) and (1.2). This includes systematic uncertainties associated to detection asymmetries, which arise because of the
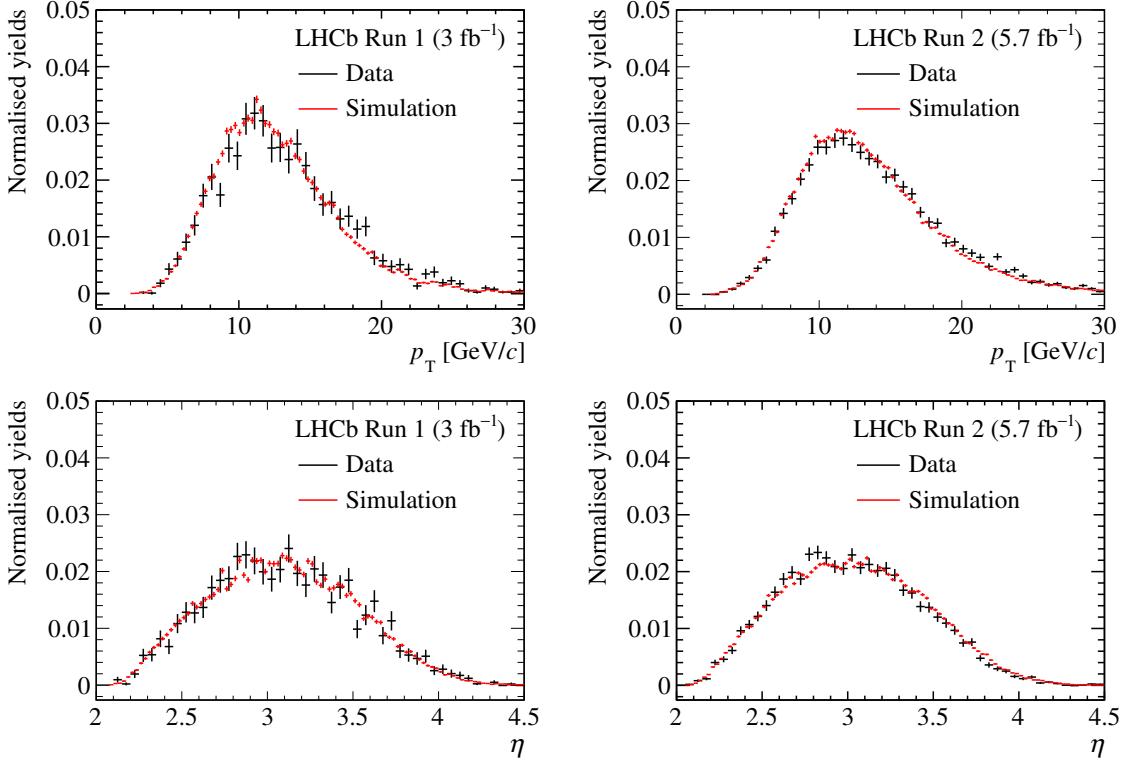
Figure 6. Distributions of (top) p_T and (bottom) η for $B^- \to \Lambda_c^+ \bar{p} \pi^-$ decays in (left) Run 1 and (right) Run 2, obtained from background-subtracted data and compared to the uncorrected distributions from simulation.

combined effect of different interaction probabilities of particles and antiparticles and the potential mismatch in the material description between data and simulation.

For the majority of measurements, the systematic uncertainties are significantly below the statistical uncertainties, as seen in table 2. Some measurements involving unobserved modes have either or both fit model and veto-related systematic uncertainties that are comparable to the statistical uncertainty, which is understood due to the size of the backgrounds in the corresponding final states. Additionally, as the statistical precision of the Run 2 measurement of $\frac{f_{\Xi_b^-}}{f_{B^-}} \cdot \frac{\mathcal{B}(\Xi_b^- \to \Lambda_c^+ K^- \pi^-)}{\mathcal{B}(B^- \to \Lambda_c^+ \bar{p} \pi^-)}$ is around 5%, it is unsurprising that its systematic uncertainties are not negligible. In particular, effects due to uncertainty in the b-hadron production kinematics are significant due to the rapid variation in efficiency with transverse momentum. These effects, however, tend to cancel in ratios where decays of the same b hadron are considered in both numerator and denominator.

In order to combine results from Run 1 and Run 2, the effects of the systematic uncertainties are considered as being either 100% correlated or completely uncorrelated between the two data-taking periods. The dominant systematic uncertainties discussed above are all correlated between Run 1 and Run 2.
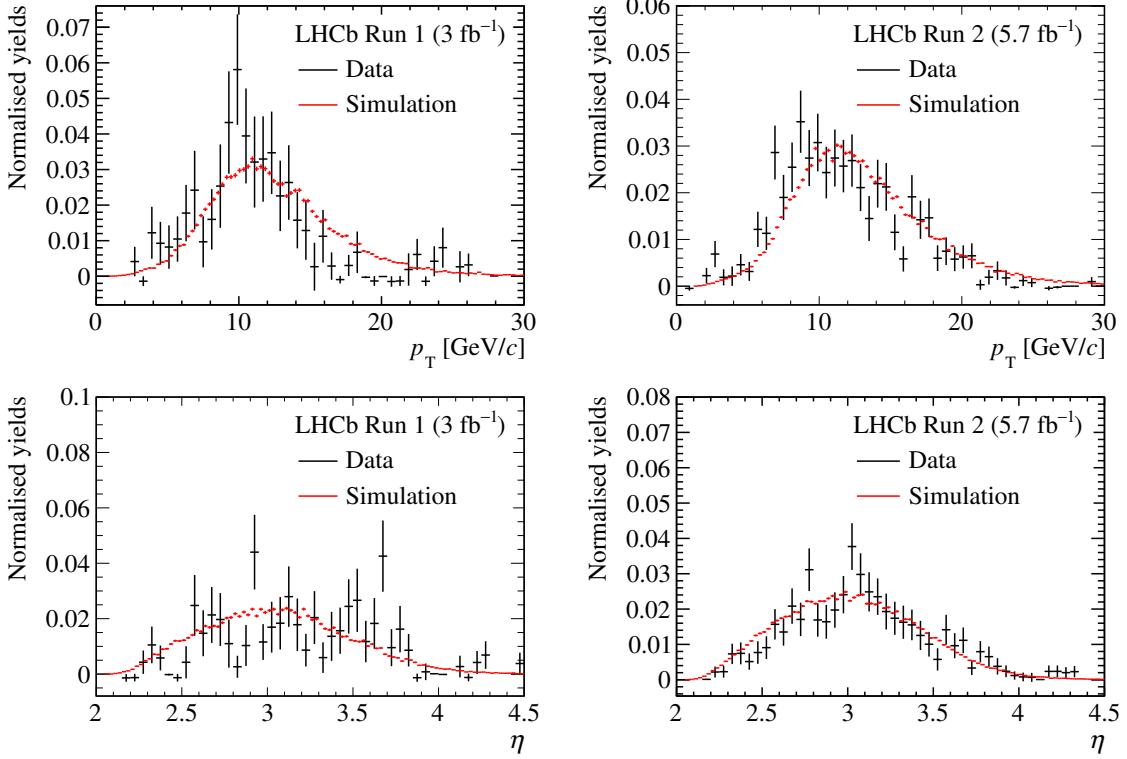
Figure 7. Distributions of (top) p_T and (bottom) η for $\Xi_b^- \to \Lambda_c^+ K^- \pi^-$ decays in (left) Run 1 and (right) Run 2, obtained from background-subtracted data and compared to the uncorrected distributions from simulation.

7 Results

Results for the ratios of fragmentation fractions and branching fractions are obtained for all channels studied relative to the $B^- \to \Lambda_c^+ \overline{p} \pi^-$ normalisation channel. In addition, since significant signals are observed for $\Xi_b^- \to \Lambda_c^+ K^- \pi^-$ and $\Omega_b^- \to \Lambda_c^+ K^- K^-$ decays, the relative branching fractions of the other Ξ_b^- and Ω_b^- decays, respectively, to those are also determined. These results are given separately for Run 1 and Run 2 in table 2.

Results for ratios of branching fractions of the same b hadron do not depend on pp collision centre-of-mass energy, and therefore the Run 1 and Run 2 results can be combined. This is done taking correlations of systematic uncertainties into account, using the method described in ref. [48], to obtain

$$\frac{\mathcal{B}\left(B^- \to \Lambda_c^+ \overline{p} K^-\right)}{\mathcal{B}\left(B^- \to \Lambda_c^+ \overline{p} \pi^-\right)} = 0.0397 \pm 0.0023\,(\text{stat}) \pm 0.0012\,(\text{syst}),$$

$$\frac{\mathcal{B}\left(\Xi_b^- \to \Lambda_c^+ K^- K^-\right)}{\mathcal{B}\left(\Xi_b^- \to \Lambda_c^+ K^- \pi^-\right)} = 0.045 \pm 0.011\,(\text{stat}) \pm 0.005\,(\text{syst}),$$

$$\frac{\mathcal{B}\left(\Xi_b^- \to \Lambda_c^+ \pi^- \pi^-\right)}{\mathcal{B}\left(\Xi_b^- \to \Lambda_c^+ K^- \pi^-\right)} = 0.025 \pm 0.013\,(\text{stat}) \pm 0.019\,(\text{syst}),$$

	Run 1	Run 2
$\dfrac{\mathcal{B}(B^-\to\Lambda_c^+\overline{p}K^-)}{\mathcal{B}(B^-\to\Lambda_c^+\overline{p}\pi^-)}$	$0.0404\pm0.0056\pm0.0021$	$0.0395\pm0.0025\pm0.0013$
$\dfrac{f_{\Xi_b^-}}{f_{B^-}}\cdot\dfrac{\mathcal{B}(\Xi_b^-\to\Lambda_c^+K^-K^-)}{\mathcal{B}(B^-\to\Lambda_c^+\overline{p}\pi^-)}$	$0.0085\pm0.0037\pm0.0024$	$0.0032\pm0.0009\pm0.0003$
$\dfrac{f_{\Xi_b^-}}{f_{B^-}}\cdot\dfrac{\mathcal{B}(\Xi_b^-\to\Lambda_c^+K^-\pi^-)}{\mathcal{B}(B^-\to\Lambda_c^+\overline{p}\pi^-)}$	$0.113\pm0.012\pm0.029$	$0.076\pm0.004\pm0.006$
$\dfrac{f_{\Xi_b^-}}{f_{B^-}}\cdot\dfrac{\mathcal{B}(\Xi_b^-\to\Lambda_c^+\pi^-\pi^-)}{\mathcal{B}(B^-\to\Lambda_c^+\overline{p}\pi^-)}$	$0.0110\pm0.0054\pm0.0057$	$0.0015\pm0.0010\pm0.0014$
$\dfrac{f_{\Omega_b^-}}{f_{B^-}}\cdot\dfrac{\mathcal{B}(\Omega_b^-\to\Lambda_c^+K^-K^-)}{\mathcal{B}(B^-\to\Lambda_c^+\overline{p}\pi^-)}$	$0.0053\pm0.0023\pm0.0012$	$0.0037\pm0.0009\pm0.0004$
$\dfrac{f_{\Omega_b^-}}{f_{B^-}}\cdot\dfrac{\mathcal{B}(\Omega_b^-\to\Lambda_c^+K^-\pi^-)}{\mathcal{B}(B^-\to\Lambda_c^+\overline{p}\pi^-)}$	$0.0020\pm0.0021\pm0.00013$	$0.0006\pm0.0005\pm0.0004$
$\dfrac{f_{\Omega_b^-}}{f_{B^-}}\cdot\dfrac{\mathcal{B}(\Omega_b^-\to\Lambda_c^+\pi^-\pi^-)}{\mathcal{B}(B^-\to\Lambda_c^+\overline{p}\pi^-)}$	$0.0013\pm0.0029\pm0.0027$	$-0.0003\pm0.0004\pm0.0005$
$\dfrac{\mathcal{B}(\Xi_b^-\to\Lambda_c^+K^-K^-)}{\mathcal{B}(\Xi_b^-\to\Lambda_c^+K^-\pi^-)}$	$0.075\pm0.034\pm0.011$	$0.041\pm0.012\pm0.005$
$\dfrac{\mathcal{B}(\Xi_b^-\to\Lambda_c^+\pi^-\pi^-)}{\mathcal{B}(\Xi_b^-\to\Lambda_c^+K^-\pi^-)}$	$0.097\pm0.049\pm0.046$	$0.019\pm0.013\pm0.017$
$\dfrac{\mathcal{B}(\Omega_b^-\to\Lambda_c^+K^-\pi^-)}{\mathcal{B}(\Omega_b^-\to\Lambda_c^+K^-K^-)}$	$0.38\pm0.43\pm0.24$	$0.17\pm0.13\pm0.09$
$\dfrac{\mathcal{B}(\Omega_b^-\to\Lambda_c^+\pi^-\pi^-)}{\mathcal{B}(\Omega_b^-\to\Lambda_c^+K^-K^-)}$	$0.24\pm0.57\pm0.53$	$-0.08\pm0.12\pm0.15$

Table 2. Ratios of branching fractions, multiplied where appropriate by ratios of fragmentation fractions, separately for Run 1 and Run 2. In each result the first uncertainty is statistical and the second is systematic.

$$\frac{\mathcal{B}\left(\Omega_b^-\to\Lambda_c^+K^-\pi^-\right)}{\mathcal{B}\left(\Omega_b^-\to\Lambda_c^+K^-K^-\right)} = 0.19\pm0.12\,(\text{stat})\pm0.10\,(\text{syst})\,,$$

$$\frac{\mathcal{B}\left(\Omega_b^-\to\Lambda_c^+\pi^-\pi^-\right)}{\mathcal{B}\left(\Omega_b^-\to\Lambda_c^+K^-K^-\right)} = -0.07\pm0.12\,(\text{stat})\pm0.16\,(\text{syst})\,,$$

where the first uncertainty is statistical and the second is systematic.

The significance of the signal in each mode is determined using Wilks' theorem, i.e. as $\sqrt{2\Delta(\text{NLL})}$ where $2\Delta(\text{NLL})$ is double the difference in negative log-likelihood obtained in the best fit (with the signal yield free) and in another fit where the relevant signal yield is fixed to zero. Significances are determined separately for Run 1 and Run 2, using the likelihood functions obtained from the fits convolved with Gaussian functions to account for relevant sources of systematic uncertainty, and then combined taking correlations of systematic uncertainties into account. As the $B^-\to\Lambda_c^+\overline{p}K^-$ and $\Xi_b^-\to\Lambda_c^+K^-\pi^-$ signals are clearly far in excess of $5\,\sigma$ significance, they are not quantified further. Similarly, as the statistical significances of the $\Xi_b^-\to\Lambda_c^+\pi^-\pi^-$, $\Omega_b^-\to\Lambda_c^+K^-\pi^-$ and $\Omega_b^-\to\Lambda_c^+\pi^-\pi^-$ signals are found to be below $3\,\sigma$, they are not quantified further. For the $\Xi_b^-\to\Lambda_c^+K^-K^-$ and $\Omega_b^-\to\Lambda_c^+K^-K^-$ channels, the combined significances are found to be above $5\,\sigma$, as shown in table 3.

For the modes where no significant signal is observed, upper limits on the relative ratios of fragmentation fractions times branching fractions are reported. The limits are obtained

Decay	Run 1	Run 2	Combined
Statistical uncertainties only			
$\Xi_b^- \to \Lambda_c^+ K^- K^-$	3.6	5.5	6.3
$\Omega_b^- \to \Lambda_c^+ K^- K^-$	4.2	7.9	8.8
Including systematic uncertainties			
$\Xi_b^- \to \Lambda_c^+ K^- K^-$	3.5	5.2	5.9
$\Omega_b^- \to \Lambda_c^+ K^- K^-$	3.6	6.9	7.5

Table 3. Significances (σ) of the signals for $\Xi_b^- \to \Lambda_c^+ K^- K^-$ and $\Omega_b^- \to \Lambda_c^+ K^- K^-$ decays.

for the combined Run 1 and Run 2 ratios, so in cases where the decays in the numerator and denominator involve different b hadrons, the ratio of fragmentation fractions in the combination should be considered as an effective average of the values for Run 1 and Run 2 (dominated by the latter due to the larger sample size). A combined likelihood for Run 1 and Run 2 is obtained, taking correlations of systematic uncertainties into account, and upper limits at 90% (95%) confidence level (CL) are determined by integrating the likelihood in the physical region of non-negative relative fragmentation fractions times branching fractions. The combined limits are

$$\frac{f_{\Xi_b^-}}{f_{B^-}} \cdot \frac{\mathcal{B}\left(\Xi_b^- \to \Lambda_c^+ \pi^- \pi^-\right)}{\mathcal{B}\left(B^- \to \Lambda_c^+ \overline{p} \pi^-\right)} < 0.0049 \,(0.0057) \text{ at } 90\% \,(95\%) \text{ CL},$$

$$\frac{f_{\Omega_b^-}}{f_{B^-}} \cdot \frac{\mathcal{B}\left(\Omega_b^- \to \Lambda_c^+ K^- \pi^-\right)}{\mathcal{B}\left(B^- \to \Lambda_c^+ \overline{p} \pi^-\right)} < 0.0019 \,(0.0022) \text{ at } 90\% \,(95\%) \text{ CL},$$

$$\frac{f_{\Omega_b^-}}{f_{B^-}} \cdot \frac{\mathcal{B}\left(\Omega_b^- \to \Lambda_c^+ \pi^- \pi^-\right)}{\mathcal{B}\left(B^- \to \Lambda_c^+ \overline{p} \pi^-\right)} < 0.0012 \,(0.0015) \text{ at } 90\% \,(95\%) \text{ CL},$$

$$\frac{\mathcal{B}\left(\Xi_b^- \to \Lambda_c^+ \pi^- \pi^-\right)}{\mathcal{B}\left(\Xi_b^- \to \Lambda_c^+ K^- \pi^-\right)} < 0.065 \,(0.074) \text{ at } 90\% \,(95\%) \text{ CL},$$

$$\frac{\mathcal{B}\left(\Omega_b^- \to \Lambda_c^+ K^- \pi^-\right)}{\mathcal{B}\left(\Omega_b^- \to \Lambda_c^+ K^- K^-\right)} < 0.56 \,(0.64) \text{ at } 90\% \,(95\%) \text{ CL},$$

$$\frac{\mathcal{B}\left(\Omega_b^- \to \Lambda_c^+ \pi^- \pi^-\right)}{\mathcal{B}\left(\Omega_b^- \to \Lambda_c^+ K^- K^-\right)} < 0.37 \,(0.45) \text{ at } 90\% \,(95\%) \text{ CL}.$$

In channels with large enough yields, namely $B^- \to \Lambda_c^+ \overline{p} \pi^-$, $B^- \to \Lambda_c^+ \overline{p} K^-$ and $\Xi_b^- \to \Lambda_c^+ K^- \pi^-$, the candidate-by-candidate efficiency correction procedure allows background-subtracted and efficiency-corrected phase-space distributions to be obtained. Two-body mass projections of these distributions are shown in figures 8, 9 and 10. Clear resonant structures are seen in $\Lambda_c^+ \pi^-$ and $\Lambda_c^+ K^-$ mass distributions, while enhancements are observed near threshold in $\Lambda_c^+ \overline{p}$ mass. The $\Lambda_c^+ \pi^-$ and $\Lambda_c^+ \overline{p}$ structures observed in $B^- \to \Lambda_c^+ \overline{p} \pi^-$ decays
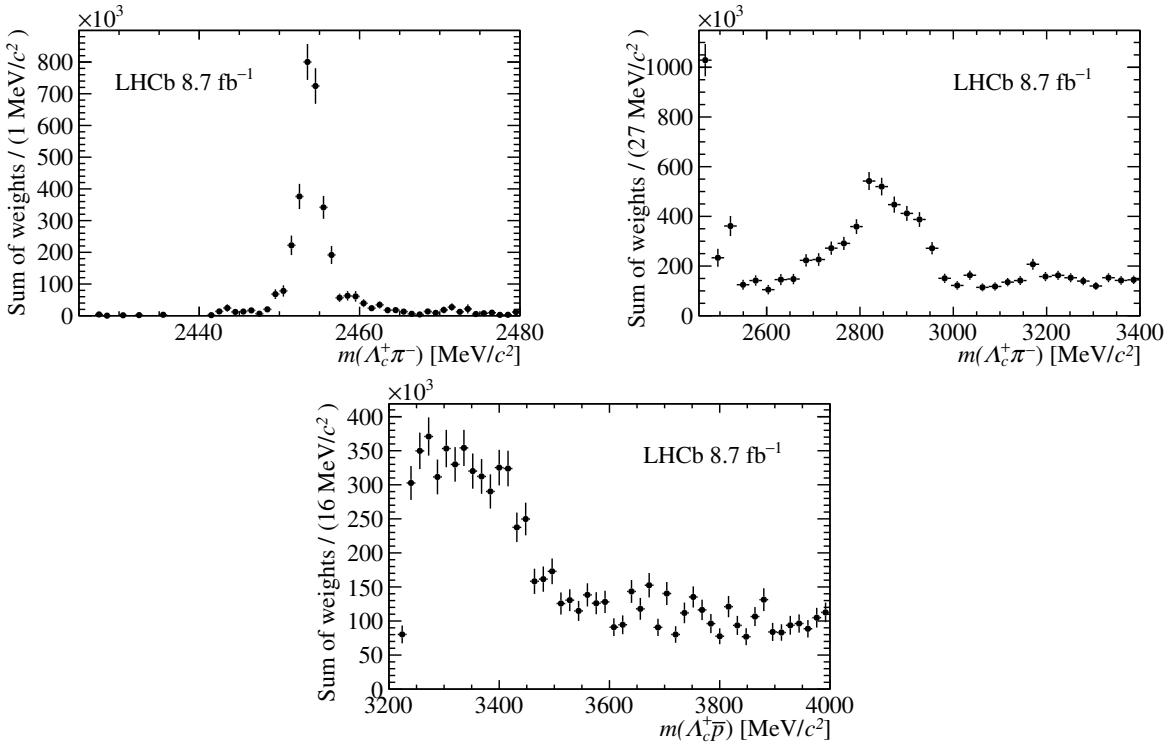
Figure 8. Background-subtracted and efficiency-corrected distributions of $B^- \to \Lambda_c^+ \overline{p} \pi^-$ decays: (top left) $m(\Lambda_c^+ \pi^-)$ at low mass, showing the $\Sigma_c(2455)^0$ resonance peak; (top right) $m(\Lambda_c^+ \pi^-)$ at higher mass, showing additional Σ_c resonance structures; (bottom) $m(\Lambda_c^+ \overline{p})$ at low mass, where $m(\Lambda_c^+ \pi^-) > 2460 \, \mathrm{MeV}/c^2$ has been required to remove contributions from the $\Sigma_c(2455)^0$ resonance.
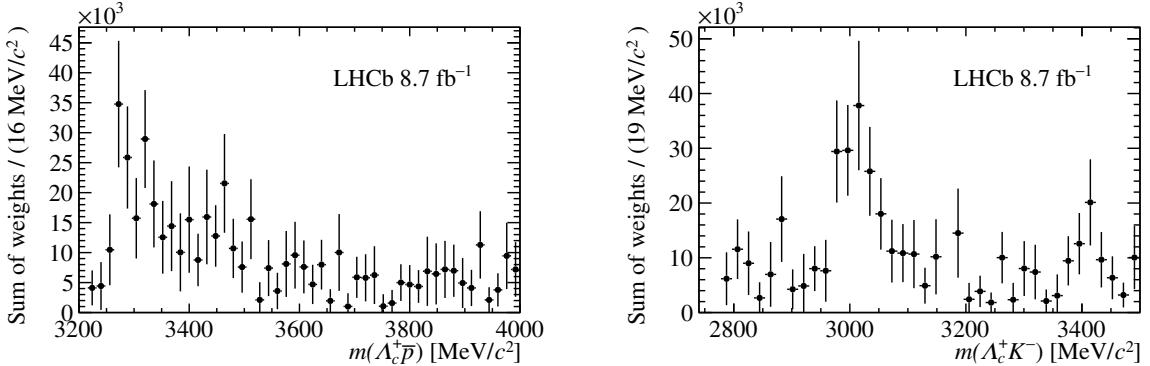
Figure 9. Background-subtracted and efficiency-corrected distributions of $B^- \to \Lambda_c^+ \overline{p} K^-$ decays: (left) $m(\Lambda_c^+ \overline{p})$ at low mass; (right) $m(\Lambda_c^+ K^-)$ at low mass, where $m(\Lambda_c^+ \overline{p}) > 3500 \, \mathrm{MeV}/c^2$ has been required to remove contributions from the $\Lambda_c^+ \overline{p}$ threshold enhancement.

appear consistent with those seen in previous studies of this decay [11, 12]. A $\Lambda_c^+ \overline{p}$ threshold enhancement is also observed in $B^- \to \Lambda_c^+ \overline{p} K^-$ decays, where $\Lambda_c^+ K^-$ resonances are also seen that may be the same as those observed in other recent studies [49, 50]. Both $\Lambda_c^+ \pi^-$ and $\Lambda_c^+ K^-$ resonances are also seen in $\Xi_b^- \to \Lambda_c^+ K^- \pi^-$ decays. Detailed investigations of these structures is beyond the scope of this work.
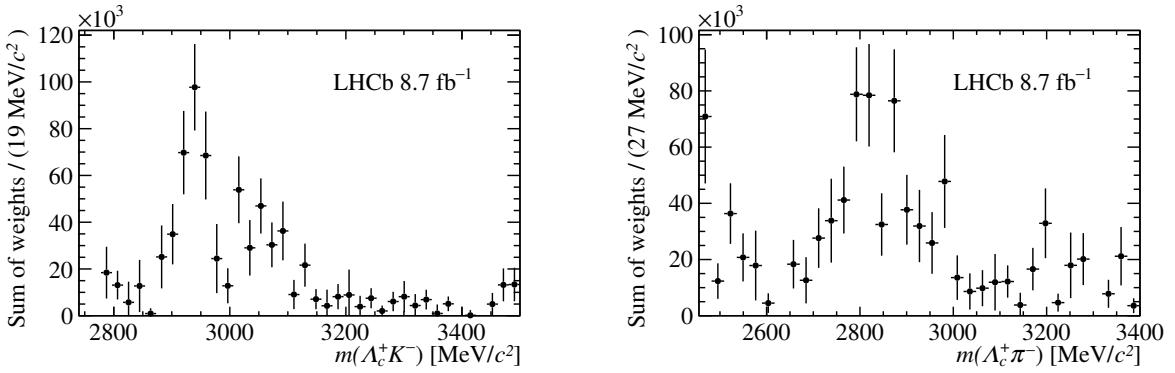
Figure 10. Background-subtracted and efficiency-corrected distributions of $\Xi_b^- \to \Lambda_c^+ K^- \pi^-$ decays: (left) $m(\Lambda_c^+ K^-)$ at low mass; (right) $m(\Lambda_c^+ \pi^-)$ at low mass.
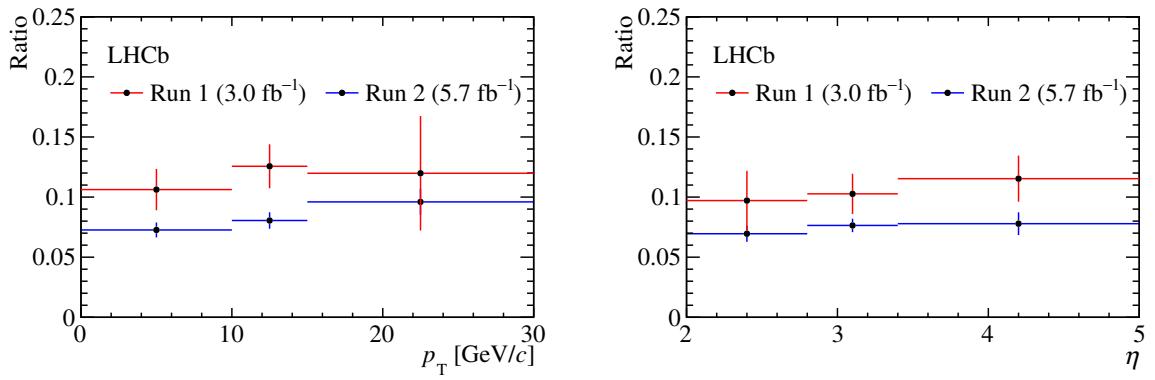
Figure 11. Variation of the ratio of fragmentation fractions times branching fractions of $\Xi_b^- \to \Lambda_c^+ K^- \pi^-$ and $B^- \to \Lambda_c^+ \overline{p} \pi^-$ decays with (left) b-hadron transverse momentum and (right) pseudorapidity, separately for Run 1 and Run 2, with statistical uncertainties only.

The reasonably large yield observed in $\Xi_b^- \to \Lambda_c^+ K^- \pi^-$ decays also allows the corresponding ratio of fragmentation fractions times branching fractions, relative to the $B^- \to \Lambda_c^+ \overline{p} \pi^-$ control channel, to be determined in intervals of the b-hadron kinematic variables. Since the ratio of branching fractions is constant, this quantity probes dependence of the ratio of fragmentation fractions on the production kinematics. Significant dependence on p_T of the Λ_b^0 and B_s^0 fragmentation fractions relative to those of B^0 and B^+ mesons, has previously been observed [51–53]. Knowledge of whether similar effects are present in the ratio of Ξ_b^- to B^- fragmentation fractions would provide insight into production mechanisms. Results are shown in figure 11, with statistical uncertainties only (the majority of systematic effects are correlated bin-to-bin and therefore not relevant to the dependence). The limited statistical precision precludes any strong conclusion, except that the Run 1 result is higher than that of Run 2, as also seen in table 2. As a cross-check, the relative branching fraction of $B^- \to \Lambda_c^+ \overline{p} K^-$ and $B^- \to \Lambda_c^+ \overline{p} \pi^-$ decays is shown in the same kinematic bins in figure 12. No dependence is seen, as expected.

Similarly, the Ξ_b^- production asymmetry is studied in intervals of b-hadron kinematics using the $\Xi_b^- \to \Lambda_c^+ K^- \pi^-$ channel, with the $B^- \to \Lambda_c^+ \overline{p} \pi^-$ mode used as a control channel.
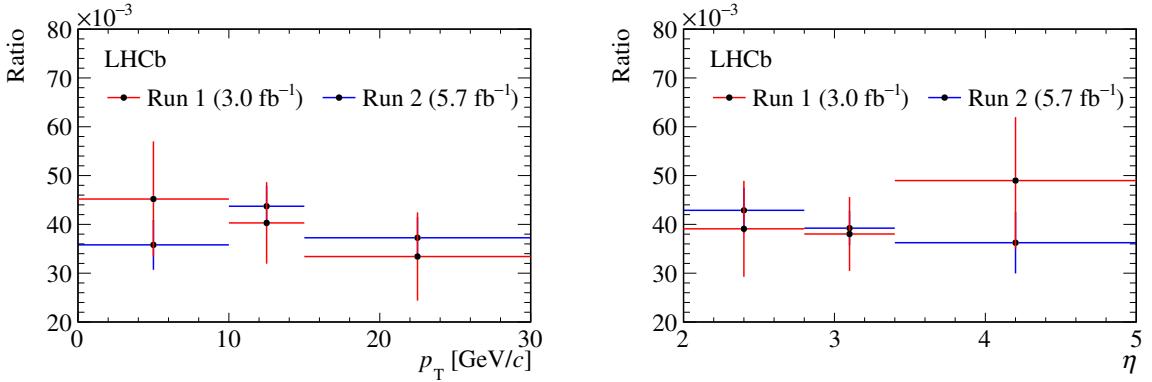
Figure 12. Variation of the ratio of branching fractions of $B^- \to \Lambda_c^+ \overline{p} K^-$ and $B^- \to \Lambda_c^+ \overline{p} \pi^-$ decays with (left) b-hadron transverse momentum and (right) pseudorapidity, separately for Run 1 and Run 2, with statistical uncertainties only.
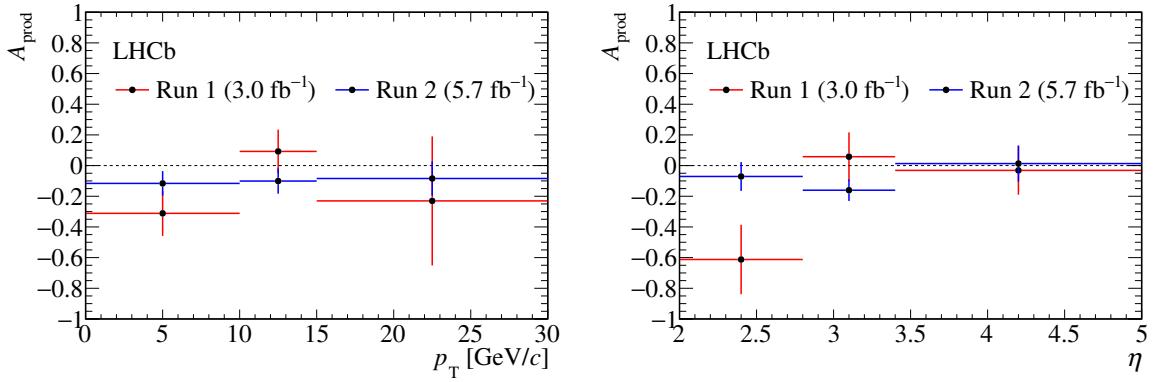

Figure 13. Variation of Ξ_b^- production asymmetry with (left) Ξ_b^- transverse momentum and (right) pseudorapidity determined with $\Xi_b^- \to \Lambda_c^+ K^- \pi^-$ decays.

The results are shown, with statistical uncertainties only, in figures 13 and 14 respectively. No strong dependence of the Ξ_b^- production asymmetry with either p_{T} or η is observed, and all results are consistent with zero asymmetry within uncertainties. This is as expected since although a significant Λ_b^0 production asymmetry, with a potential dependence on kinematics, has been observed [45], the effect is at the level of 2% or smaller and hence a comparably sized asymmetry would not be detectable in the current analysis. The results for the Ξ_b^- production asymmetry in pp collisions, integrated over the LHCb acceptance, are

$$\mathcal{A}_{\mathrm{prod}}(\Xi_b^-; \mathrm{Run}\ 1) = -0.10 \pm 0.10\,(\mathrm{stat}) \pm 0.03\,(\mathrm{syst})\,,$$
$$\mathcal{A}_{\mathrm{prod}}(\Xi_b^-; \mathrm{Run}\ 2) = -0.10 \pm 0.05\,(\mathrm{stat}) \pm 0.02\,(\mathrm{syst})\,,$$

which are also consistent with zero and with previous measurements of the Ξ_b^- production asymmetry [10]. The control channel results are seen to be consistent with zero and with previous measurements of the B^- production asymmetry in pp collisions in the LHCb acceptance [54, 55].
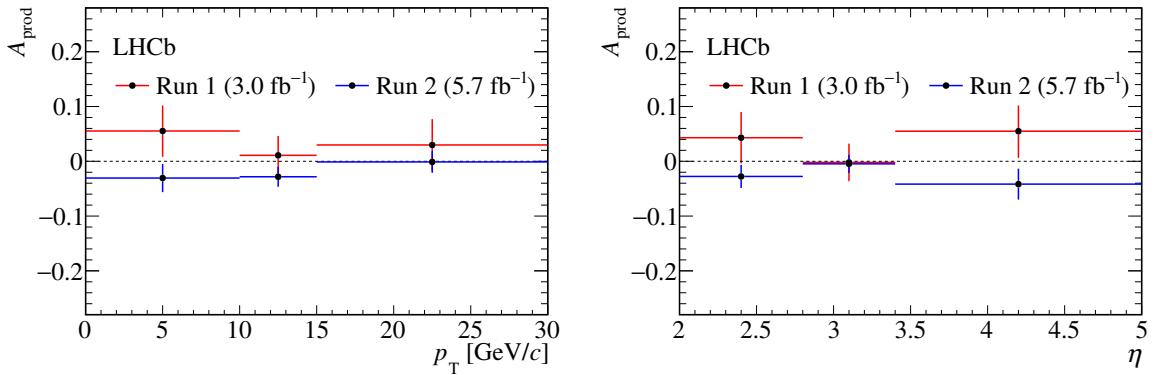
Figure 14. Variation of B^- production asymmetry with (left) B^- transverse momentum and (right) pseudorapidity determined with the $B^- \to \Lambda_c^+ \overline{p} \pi^-$ control mode.

8 Conclusion

The decays $\Xi_b^- \to \Lambda_c^+ h^- h'^-$ and $\Omega_b^- \to \Lambda_c^+ h^- h'^-$, with $h^- h'^-$ being $\pi^- \pi^-$, $K^- \pi^-$ and $K^- K^-$ are studied using a data sample of pp collisions corresponding to an integrated luminosity of $8.7\,\text{fb}^{-1}$ collected by LHCb during the Run 1 and Run 2 operation periods of the LHC. The $\Xi_b^- \to \Lambda_c^+ K^- \pi^-$ mode is observed with large significance, and the $\Xi_b^- \to \Lambda_c^+ K^- K^-$ and $\Omega_b^- \to \Lambda_c^+ K^- K^-$ modes are also observed with over $5\,\sigma$ significance. Ratios of fragmentation fractions times branching fractions are determined for all channels relative to the control mode $B^- \to \Lambda_c^+ \overline{p} \pi^-$, and additionally ratios of branching fractions are determined relative to the most significant decay for each b baryon. The $\Xi_b^- \to \Lambda_c^+ K^- \pi^-$ mode is also used to study the variation with kinematics of the Ξ_b^-/B^- production ratio, and the Ξ_b^- production asymmetry. In both cases the variation is found to be consistent with zero; the integrated Ξ_b^- production asymmetry within the LHCb acceptance is also found to be consistent with zero. Furthermore, the $B^- \to \Lambda_c^+ \overline{p} K^-$ decay is observed with large significance, and its branching fraction measured relative to that of the $B^- \to \Lambda_c^+ \overline{p} \pi^-$ control mode.

These results significantly increase the currently available experimental knowledge of Ξ_b^- and Ω_b^- decays. The decay modes observed can in future be used to improve knowledge of the processes behind b-baryon production in high-energy pp collisions, including production asymmetries, and to study charm baryon spectroscopy.

References

[1] LHCb collaboration, *Measurement of the mass and lifetime of the Ω_b^- baryon*, *Phys. Rev. D* **93** (2016) 092007 [arXiv:1604.01412] [InSPIRE].

[2] LHCb collaboration, *Observation of the decay $\Xi_b^- \to pK^-K^-$*, *Phys. Rev. Lett.* **118** (2017) 071801 [arXiv:1612.02244] [InSPIRE].

[3] LHCb collaboration, *Observation of the $\Xi_b^- \to J/\psi \Lambda K^-$ decay*, *Phys. Lett. B* **772** (2017) 265 [arXiv:1701.05274] [InSPIRE].

[4] LHCb collaboration, *Search for CP violation in $\Xi_b^- \to pK^-K^-$ decays*, *Phys. Rev. D* **104** (2021) 052010 [arXiv:2104.15074] [InSPIRE].

[5] LHCb collaboration, *Observation of excited Ω_c^0 baryons in $\Omega_b^- \to \Xi_c^+ K^- \pi^-$ decays*, *Phys. Rev. D* **104** (2021) L091102 [arXiv:2107.03419] [InSPIRE].

[6] LHCb collaboration, *Measurement of the mass difference and relative production rate of the Ω_b^- and Ξ_b^- baryons*, *Phys. Rev. D* **108** (2023) 052008 [arXiv:2305.15329] [InSPIRE].

[7] LHCb collaboration, *Observation of new baryons in the $\Xi_b^- \pi^+ \pi^-$ and $\Xi_b^0 \pi^+ \pi^-$ systems*, *Phys. Rev. Lett.* **131** (2023) 171901 [arXiv:2307.13399] [InSPIRE].

[8] LHCb collaboration, *Observation and branching fraction measurement of the decay $\Xi_b^- \to \Lambda_b^0 \pi^-$*, *Phys. Rev. D* **108** (2023) 072002 [arXiv:2307.09427] [InSPIRE].

[9] CMS collaboration, *Observation of the $\Xi_b^- \to \psi(2S)\Xi^-$ decay and studies of the Ξ_b^{*0} baryon in proton-proton collisions at $\sqrt{s} = 13$ TeV*, *Phys. Rev. D* **110** (2024) 012002 [arXiv:2402.17738] [InSPIRE].

[10] LHCb collaboration, *Measurement of the mass and production rate of Ξ_b^- baryons*, *Phys. Rev. D* **99** (2019) 052006 [arXiv:1901.07075] [InSPIRE].

[11] BELLE collaboration, *Study of decay mechanisms in $B^- \to \Lambda_c^+ \bar{p}\pi^-$ decays and observation of low-mass structure in the $\Lambda_c^+ \bar{p}$ system*, *Phys. Rev. Lett.* **97** (2006) 242001 [hep-ex/0409005] [InSPIRE].

[12] BaBar collaboration, *Measurements of $\mathcal{B}(\overline{B}^0 \to \Lambda_c^+ \overline{p})$ and $\mathcal{B}(B^- \to \Lambda_c^+ \overline{p}\pi^-)$ and studies of $\Lambda_c^+ \pi^-$ resonances*, *Phys. Rev. D* **78** (2008) 112003 [`arXiv:0807.4974`] [INSPIRE].

[13] M. Pivk and F.R. Le Diberder, *SPlot: a statistical tool to unfold data distributions*, *Nucl. Instrum. Meth. A* **555** (2005) 356 [`physics/0402083`] [INSPIRE].

[14] LHCb collaboration, *The LHCb detector at the LHC*, 2008 *JINST* **3** S08005 [INSPIRE].

[15] LHCb collaboration, *LHCb detector performance*, *Int. J. Mod. Phys. A* **30** (2015) 1530022 [`arXiv:1412.6352`] [INSPIRE].

[16] R. Aaij et al., *Performance of the LHCb vertex locator*, 2014 *JINST* **9** P09007 [`arXiv:1405.7808`] [INSPIRE].

[17] LHCb Outer Tracker Group collaboration, *Performance of the LHCb outer tracker*, 2014 *JINST* **9** P01002 [`arXiv:1311.3893`] [INSPIRE].

[18] LHCb Outer Tracker Group collaboration, *Improved performance of the LHCb outer tracker in LHC run 2*, 2017 *JINST* **12** P11016 [`arXiv:1708.00819`] [INSPIRE].

[19] LHCb RICH Group collaboration, *Performance of the LHCb RICH detector at the LHC*, *Eur. Phys. J. C* **73** (2013) 2431 [`arXiv:1211.6759`] [INSPIRE].

[20] A.A. Alves Jr. et al., *Performance of the LHCb muon system*, 2013 *JINST* **8** P02022 [`arXiv:1211.1346`] [INSPIRE].

[21] R. Aaij et al., *The LHCb trigger and its performance in 2011*, 2013 *JINST* **8** P04022 [`arXiv:1211.3055`] [INSPIRE].

[22] LHCb collaboration, *Design and performance of the LHCb trigger and full real-time reconstruction in run 2 of the LHC*, 2019 *JINST* **14** P04013 [`arXiv:1812.10790`] [INSPIRE].

[23] V.V. Gligorov and M. Williams, *Efficient, reliable and fast high-level triggering using a bonsai boosted decision tree*, 2013 *JINST* **8** P02013 [`arXiv:1210.6861`] [INSPIRE].

[24] T. Likhomanenko et al., *LHCb topological trigger reoptimization*, *J. Phys. Conf. Ser.* **664** (2015) 082025 [`arXiv:1510.00572`] [INSPIRE].

[25] T. Sjostrand, S. Mrenna and P.Z. Skands, *A brief introduction to PYTHIA 8.1*, *Comput. Phys. Commun.* **178** (2008) 852 [`arXiv:0710.3820`] [INSPIRE].

[26] T. Sjostrand, S. Mrenna and P.Z. Skands, *PYTHIA 6.4 physics and manual*, *JHEP* **05** (2006) 026 [`hep-ph/0603175`] [INSPIRE].

[27] LHCb collaboration, *Handling of the generation of primary events in Gauss, the LHCb simulation framework*, *J. Phys. Conf. Ser.* **331** (2011) 032047 [INSPIRE].

[28] D.J. Lange, *The EvtGen particle decay simulation package*, *Nucl. Instrum. Meth. A* **462** (2001) 152 [INSPIRE].

[29] N. Davidson, T. Przedzinski and Z. Was, *PHOTOS interface in C++: technical and physics documentation*, *Comput. Phys. Commun.* **199** (2016) 86 [`arXiv:1011.0937`] [INSPIRE].

[30] J. Allison et al., *GEANT4 developments and applications*, *IEEE Trans. Nucl. Sci.* **53** (2006) 270 [INSPIRE].

[31] GEANT4 collaboration, *GEANT4 — a simulation toolkit*, *Nucl. Instrum. Meth. A* **506** (2003) 250 [INSPIRE].

[32] LHCb collaboration, *The LHCb simulation application, Gauss: design, evolution and experience*, *J. Phys. Conf. Ser.* **331** (2011) 032023 [INSPIRE].

[33] D. Müller, M. Clemencic, G. Corti and M. Gersabeck, *ReDecay: a novel approach to speed up the simulation at LHCb*, *Eur. Phys. J. C* **78** (2018) 1009 [arXiv:1810.10362] [INSPIRE].

[34] R. Aaij et al., *Selection and processing of calibration samples to measure the particle identification performance of the LHCb experiment in run 2*, *EPJ Tech. Instrum.* **6** (2019) 1 [arXiv:1803.00824] [INSPIRE].

[35] T. Chen and C. Guestrin, *XGBoost: a scalable tree boosting system*, in *Proceedings of the* 22nd *ACM SIGKDD international conference on knowledge discovery and data mining*, KDD '16, ACM, August 2016 [DOI:10.1145/2939672.2939785] [arXiv:1603.02754] [INSPIRE].

[36] LHCb collaboration, *Observation of CP violation in $B^{\pm} \to DK^{\pm}$ decays*, *Phys. Lett. B* **712** (2012) 203 [*Erratum ibid.* **713** (2012) 351] [arXiv:1203.3662] [INSPIRE].

[37] G. Punzi, *Sensitivity of searches for new signals and its optimization*, *eConf C* **030908** (2003) MODT002 [physics/0308063] [INSPIRE].

[38] T. Skwarnicki, *A study of the radiative CASCADE transitions between the Upsilon-Prime and Upsilon resonances*, Ph.D. thesis, INP, Cracow, Poland (1986) [INSPIRE].

[39] G.A. Cowan, D.C. Craik and M.D. Needham, *RapidSim: an application for the fast simulation of heavy-quark hadron decays*, *Comput. Phys. Commun.* **214** (2017) 239 [arXiv:1612.07489] [INSPIRE].

[40] K.S. Cranmer, *Kernel estimation in high-energy physics*, *Comput. Phys. Commun.* **136** (2001) 198 [hep-ex/0011057] [INSPIRE].

[41] J. Back et al., *LAURA^{++}: a Dalitz plot fitter*, *Comput. Phys. Commun.* **231** (2018) 198 [arXiv:1711.09854] [INSPIRE].

[42] CDF collaboration, *Mass and lifetime measurements of bottom and charm baryons in $p\bar{p}$ collisions at $\sqrt{s} = 1.96$ TeV*, *Phys. Rev. D* **89** (2014) 072014 [arXiv:1403.8126] [INSPIRE].

[43] LHCb collaboration, *Measurement of the Ξ_b^- and Ω_b^- baryon lifetimes*, *Phys. Lett. B* **736** (2014) 154 [arXiv:1405.1543] [INSPIRE].

[44] LHCb collaboration, *Measurement of the track reconstruction efficiency at LHCb*, 2015 *JINST* **10** P02007 [arXiv:1408.1251] [INSPIRE].

[45] LHCb collaboration, *Observation of a $\Lambda_b^0 - \overline{\Lambda}_b^0$ production asymmetry in proton-proton collisions at $\sqrt{s} = 7$ and 8 TeV*, *JHEP* **10** (2021) 060 [arXiv:2107.09593] [INSPIRE].

[46] C. Abellán Beteta et al., *Calibration and performance of the LHCb calorimeters in run 1 and 2 at the LHC*, arXiv:2008.11556 [INSPIRE].

[47] LHCb collaboration, *Amplitude analysis of the $\Lambda_c^+ \to pK^-\pi^+$ decay and Λ_c^+ baryon polarization measurement in semileptonic beauty hadron decays*, *Phys. Rev. D* **108** (2023) 012023 [arXiv:2208.03262] [INSPIRE].

[48] LHCb collaboration, *Observation of the $B^0 \to \overline{D}^{*0}K^+\pi^-$ and $B_s^0 \to \overline{D}^{*0}K^-\pi^+$ decays*, *Phys. Rev. D* **105** (2022) 072005 [arXiv:2112.11428] [INSPIRE].

[49] LHCb collaboration, *Observation of new Ξ_c^0 baryons decaying to $\Lambda_c^+K^-$*, *Phys. Rev. Lett.* **124** (2020) 222001 [arXiv:2003.13649] [INSPIRE].

[50] LHCb collaboration, *Study of the $B^- \to \Lambda_c^+\bar{\Lambda}_c^-K^-$ decay*, *Phys. Rev. D* **108** (2023) 012020 [arXiv:2211.00812] [INSPIRE].

[51] LHCb collaboration, *Measurement of b hadron fractions in 13 TeV pp collisions*, *Phys. Rev. D* **100** (2019) 031102 [arXiv:1902.06794] [INSPIRE].

[52] LHCb collaboration, *Measurement of f_s/f_u variation with proton-proton collision energy and B-meson kinematics*, *Phys. Rev. Lett.* **124** (2020) 122002 [arXiv:1910.09934] [INSPIRE].

[53] LHCb collaboration, *Precise measurement of the f_s/f_d ratio of fragmentation fractions and of B_s^0 decay branching fractions*, *Phys. Rev. D* **104** (2021) 032005 [arXiv:2103.06810] [INSPIRE].

[54] LHCb collaboration, *Measurement of the $B^\pm$ production asymmetry and the CP asymmetry in $B^\pm \to J/\psi K^\pm$ decays*, *Phys. Rev. D* **95** (2017) 052005 [arXiv:1701.05501] [INSPIRE].

[55] LHCb collaboration, *Measurement of B^0, B_s^0, B^+ and Λ_b^0 production asymmetries in 7 and 8 TeV proton-proton collisions*, *Phys. Lett. B* **774** (2017) 139 [arXiv:1703.08464] [INSPIRE].

The LHCb collaboration

R. Aaij [36], A.S.W. Abdelmotteleb [55], C. Abellan Beteta [49], F. Abudinén [55], T. Ackernley [59], A. A. Adefisoye [67], B. Adeva [45], M. Adinolfi [53], P. Adlarson [79], C. Agapopoulou [13], C.A. Aidala [80], Z. Ajaltouni [11], S. Akar [64], K. Akiba [36], P. Albicocco [26], J. Albrecht [18], F. Alessio [47], M. Alexander [58], Z. Aliouche [61], P. Alvarez Cartelle [54], R. Amalric [15], S. Amato [3], J.L. Amey [53], Y. Amhis [13,47], L. An [6], L. Anderlini [25], M. Andersson [49], A. Andreianov [42], P. Andreola [49], M. Andreotti [24], D. Andreou [67], A. Anelli [29,p], D. Ao [7], F. Archilli [35,v], M. Argenton [24], S. Arguedas Cuendis [9], A. Artamonov [42], M. Artuso [67], E. Aslanides [12], R. Ataide Da Silva [48], M. Atzeni [63], B. Audurier [14], D. Bacher [62], I. Bachiller Perea [10], S. Bachmann [20], M. Bachmayer [48], J.J. Back [55], P. Baladron Rodriguez [45], V. Balagura [14], W. Baldini [24], H. Bao [7], J. Baptista de Souza Leite [59], M. Barbetti [25,m], I. R. Barbosa [68], R.J. Barlow [61], M. Barnyakov [23], S. Barsuk [13], W. Barter [57], M. Bartolini [54], J. Bartz [67], J.M. Basels [16], G. Bassi [33,s], B. Batsukh [5], A. Bay [48], A. Beck [55], M. Becker [18], F. Bedeschi [33], I.B. Bediaga [2], S. Belin [45], V. Bellee [49], K. Belous [42], I. Belov [27], I. Belyaev [34], G. Benane [12], G. Bencivenni [26], E. Ben-Haim [15], A. Berezhnoy [42], R. Bernet [49], S. Bernet Andres [43], A. Bertolin [31], C. Betancourt [49], F. Betti [57], J. Bex [54], Ia. Bezshyiko [49], J. Bhom [39], M.S. Bieker [18], N.V. Biesuz [24], P. Billoir [15], A. Biolchini [36], M. Birch [60], F.C.R. Bishop [10], A. Bitadze [61], A. Bizzeti , T. Blake [55], F. Blanc [48], J.E. Blank [18], S. Blusk [67], V. Bocharnikov [42], J.A. Boelhauve [18], O. Boente Garcia [14], T. Boettcher [64], A. Bohare [57], A. Boldyrev [42], C.S. Bolognani [76], R. Bolzonella [24,l], N. Bondar [42], F. Borgato [31,q], S. Borghi [61], M. Borsato [29,p], J.T. Borsuk [39], S.A. Bouchiba [48], T.J.V. Bowcock [59], A. Boyer [47], C. Bozzi [24], A. Brea Rodriguez [48], N. Breer [18], J. Brodzicka [39], A. Brossa Gonzalo [45], J. Brown [59], D. Brundu [30], E. Buchanan [57], A. Buonaura [49], L. Buonincontri [31,q], A.T. Burke [61], C. Burr [47], A. Butkevich [42], J.S. Butter [54], J. Buytaert [47], W. Byczynski [47], S. Cadeddu [30], H. Cai [72], R. Calabrese [24,l], S. Calderon Ramirez [9], L. Calefice [44], S. Cali [26], M. Calvi [29,p], M. Calvo Gomez [43], P. Camargo Magalhaes [2,z], J. I. Cambon Bouzas [45], P. Campana [26], D.H. Campora Perez [76], A.F. Campoverde Quezada [7], S. Capelli [29], L. Capriotti [24], R. Caravaca-Mora [9], A. Carbone [23,j], L. Carcedo Salgado [45], R. Cardinale [27,n], A. Cardini [30], P. Carniti [29,p], L. Carus [20], A. Casais Vidal [63], R. Caspary [20], G. Casse [59], J. Castro Godinez [9], M. Cattaneo [47], G. Cavallero [24,47], V. Cavallini [24,l], S. Celani [20], D. Cervenkov [62], S. Cesare [28,o], A.J. Chadwick [59], I. Chahrour [80], M. Charles [15], Ph. Charpentier [47], E. Chatzianagnostou [36], C.A. Chavez Barajas [59], M. Chefdeville [10], C. Chen [12], S. Chen [5], Z. Chen [7], A. Chernov [39], S. Chernyshenko [51], V. Chobanova [78], S. Cholak [48], M. Chrzaszcz [39], A. Chubykin [42], V. Chulikov [42], P. Ciambrone [26], X. Cid Vidal [45], G. Ciezarek [47], P. Cifra [47], P.E.L. Clarke [57], M. Clemencic [47], H.V. Cliff [54], J. Closier [47], C. Cocha Toapaxi [20], V. Coco [47], J. Cogan [12], E. Cogneras [11], L. Cojocariu [41], P. Collins [47], T. Colombo [47], A. Comerma-Montells [44], L. Congedo [22], A. Contu [30], N. Cooke [58], I. Corredoira [45], A. Correia [15], G. Corti [47], J.J. Cottee Meldrum [53], B. Couturier [47], D.C. Craik [49], M. Cruz Torres [2,g], E. Curras Rivera [48], R. Currie [57], C.L. Da Silva [66], S. Dadabaev [42], L. Dai [69], X. Dai [6], E. Dall'Occo [18], J. Dalseno [45], C. D'Ambrosio [47], J. Daniel [11], A. Danilina [42], P. d'Argent [22], A. Davidson [55], J.E. Davies [61], A. Davis [61],

O. De Aguiar Francisco [61], C. De Angelis [30,k], F. De Benedetti [47], J. de Boer [36],
K. De Bruyn [75], S. De Capua [61], M. De Cian [20,47], U. De Freitas Carneiro Da Graca [2,b],
E. De Lucia [26], J.M. De Miranda [2], L. De Paula [3], M. De Serio [22,h], P. De Simone [26],
F. De Vellis [18], J.A. de Vries [76], F. Debernardis [22], D. Decamp [10], V. Dedu [12],
L. Del Buono [15], B. Delaney [63], H.-P. Dembinski [18], J. Deng [8], V. Denysenko [49],
O. Deschamps [11], F. Dettori [30,k], B. Dey [74], P. Di Nezza [26], I. Diachkov [42], S. Didenko [42],
S. Ding [67], L. Dittmann [20], V. Dobishuk [51], A. D. Docheva [58], C. Dong [4], A.M. Donohoe [21],
F. Dordei [30], A.C. dos Reis [2], A. D. Dowling [67], W. Duan [70], P. Duda [77], M.W. Dudek [39],
L. Dufour [47], V. Duk [32], P. Durante [47], M. M. Duras [77], J.M. Durham [66], O. D. Durmus [74],
A. Dziurda [39], A. Dzyuba [42], S. Easo [56], E. Eckstein [17], U. Egede [1], A. Egorychev [42],
V. Egorychev [42], S. Eisenhardt [57], E. Ejopu [61], L. Eklund [79], M. Elashri [64], J. Ellbracht [18],
S. Ely [60], A. Ene [41], E. Epple [64], J. Eschle [67], S. Esen [20], T. Evans [61], F. Fabiano [30,k],
L.N. Falcao [2], Y. Fan [7], B. Fang [72], L. Fantini [32,r,47], M. Faria [48], K. Farmer [57],
D. Fazzini [29,p], L. Felkowski [77], M. Feng [5,7], M. Feo [18,47], A. Fernandez Casani [46],
M. Fernandez Gomez [45], A.D. Fernez [65], F. Ferrari [23], F. Ferreira Rodrigues [3], M. Ferrillo [49],
M. Ferro-Luzzi [47], S. Filippov [42], R.A. Fini [22], M. Fiorini [24,l], K.M. Fischer [62],
D.S. Fitzgerald [80], C. Fitzpatrick [61], F. Fleuret [14], M. Fontana [23], L. F. Foreman [61],
R. Forty [47], D. Foulds-Holt [54], M. Franco Sevilla [65], M. Frank [47], E. Franzoso [24,l],
G. Frau [61], C. Frei [47], D.A. Friday [61], J. Fu [7], Q. Fuehring [18], Y. Fujii [1], T. Fulghesu [15],
E. Gabriel [36], G. Galati [22], M.D. Galati [36], A. Gallas Torreira [45], D. Galli [23,j],
S. Gambetta [57], M. Gandelman [3], P. Gandini [28], B. Ganie [61], H. Gao [7], R. Gao [62],
Y. Gao [8], Y. Gao [6], Y. Gao[8], M. Garau [30,k], L.M. Garcia Martin [48], P. Garcia Moreno [44],
J. García Pardiñas [47], K. G. Garg [8], L. Garrido [44], C. Gaspar [47], R.E. Geertsema [36],
L.L. Gerken [18], E. Gersabeck [61], M. Gersabeck [61], T. Gershon [55], Z. Ghorbanimoghaddam[53],
L. Giambastiani [31,q], F. I. Giasemis [15,e], V. Gibson [54], H.K. Giemza [40], A.L. Gilman [62],
M. Giovannetti [26], A. Gioventù [44], L. Girardey [61], P. Gironella Gironell [44], C. Giugliano [24,l],
M.A. Giza [39], E.L. Gkougkousis [60], F.C. Glaser [13,20], V.V. Gligorov [15,47], C. Göbel [68],
E. Golobardes [43], D. Golubkov [42], A. Golutvin [60,42,47], A. Gomes [2,a,†],
S. Gomez Fernandez [44], F. Goncalves Abrantes [62], M. Goncerz [39], G. Gong [4], J.
A. Gooding [18], I.V. Gorelov [42], C. Gotti [29], J.P. Grabowski [17], L.A. Granado Cardoso [47],
E. Graugés [44], E. Graverini [48,t], L. Grazette [55], G. Graziani [], A. T. Grecu [41],
L.M. Greeven [36], N.A. Grieser [64], L. Grillo [58], S. Gromov [42], C. Gu [14], M. Guarise [24],
M. Guittiere [13], V. Guliaeva [42], P. A. Günther [20], A.-K. Guseinov [48], E. Gushchin [42],
Y. Guz [6,42,47], T. Gys [47], K. Habermann [17], T. Hadavizadeh [1], C. Hadjivasiliou [65],
G. Haefeli [48], C. Haen [47], J. Haimberger [47], M. Hajheidari[47], M.M. Halvorsen [47],
P.M. Hamilton [65], J. Hammerich [59], Q. Han [8], X. Han [20], S. Hansmann-Menzemer [20],
L. Hao [7], N. Harnew [62], M. Hartmann [13], J. He [7,c], F. Hemmer [47], C. Henderson [64],
R.D.L. Henderson [1,55], A.M. Hennequin [47], K. Hennessy [59], L. Henry [48], J. Herd [60],
P. Herrero Gascon [20], J. Heuel [16], A. Hicheur [3], G. Hijano Mendizabal[49], D. Hill [48],
S.E. Hollitt [18], J. Horswill [61], R. Hou [8], Y. Hou [11], N. Howarth[59], J. Hu[20], J. Hu [70],
W. Hu [6], X. Hu [4], W. Huang [7], W. Hulsbergen [36], R.J. Hunter [55], M. Hushchyn [42],
D. Hutchcroft [59], D. Ilin [42], P. Ilten [64], A. Inglessi [42], A. Iniukhin [42], A. Ishteev [42],
K. Ivshin [42], R. Jacobsson [47], H. Jage [16], S.J. Jaimes Elles [46,73], S. Jakobsen [47], E. Jans [36],

B.K. Jashal [46], A. Jawahery [65,47], V. Jevtic [18], E. Jiang [65], X. Jiang [5,7], Y. Jiang [7], Y. J. Jiang [6], M. John [62], D. Johnson [52], C.R. Jones [54], T.P. Jones [55], S. Joshi [40], B. Jost [47], N. Jurik [47], I. Juszczak [39], D. Kaminaris [48], S. Kandybei [50], M. Kane [57], Y. Kang [4], C. Kar [11], M. Karacson [47], D. Karpenkov [42], A. Kauniskangas [48], J.W. Kautz [64], F. Keizer [47], M. Kenzie [54], T. Ketel [36], B. Khanji [67], A. Kharisova [42], S. Kholodenko [33,47], G. Khreich [13], T. Kirn [16], V.S. Kirsebom [29,p], O. Kitouni [63], S. Klaver [37], N. Kleijne [33,s], K. Klimaszewski [40], M.R. Kmiec [40], S. Koliiev [51], L. Kolk [18], A. Konoplyannikov [42], P. Kopciewicz [38,47], P. Koppenburg [36], M. Korolev [42], I. Kostiuk [36], O. Kot[51], S. Kotriakhova [], A. Kozachuk [42], P. Kravchenko [42], L. Kravchuk [42], M. Kreps [55], P. Krokovny [42], W. Krupa [67], W. Krzemien [40], O.K. Kshyvanskyi[51], J. Kubat[20], S. Kubis [77], M. Kucharczyk [39], V. Kudryavtsev [42], E. Kulikova [42], A. Kupsc [79], B. K. Kutsenko [12], D. Lacarrere [47], A. Lai [30], A. Lampis [30], D. Lancierini [54], C. Landesa Gomez [45], J.J. Lane [1], R. Lane [53], C. Langenbruch [20], J. Langer [18], O. Lantwin [42], T. Latham [55], F. Lazzari [33,t], C. Lazzeroni [52], R. Le Gac [12], R. Lefèvre [11], A. Leflat [42], S. Legotin [42], M. Lehuraux [55], E. Lemos Cid [47], O. Leroy [12], T. Lesiak [39], B. Leverington [20], A. Li [4], H. Li [70], K. Li [8], L. Li [61], P. Li [47], P.-R. Li [71], Q. Li [5,7], S. Li [8], T. Li [5,d], T. Li [70], Y. Li[8], Y. Li [5], Z. Lian [4], X. Liang [67], S. Libralon [46], C. Lin [7], T. Lin [56], R. Lindner [47], V. Lisovskyi [48], R. Litvinov [30,47], F. L. Liu [1], G. Liu [70], K. Liu [71], S. Liu [5,7], Y. Liu [57], Y. Liu[71], Y. L. Liu [60], A. Lobo Salvia [44], A. Loi [30], J. Lomba Castro [45], T. Long [54], J.H. Lopes [3], A. Lopez Huertas [44], S. López Soliño [45], C. Lucarelli [25,m], D. Lucchesi [31,q], M. Lucio Martinez [76], V. Lukashenko [36,51], Y. Luo [6], A. Lupato [31,i], E. Luppi [24,l], K. Lynch [21], X.-R. Lyu [7], G. M. Ma [4], R. Ma [7], S. Maccolini [18], F. Machefert [13], F. Maciuc [41], B. Mack [67], I. Mackay [62], L. M. Mackey [67], L.R. Madhan Mohan [54], M.J. Madurai [52], A. Maevskiy [42], D. Magdalinski [36], D. Maisuzenko [42], M.W. Majewski[38], J.J. Malczewski [39], S. Malde [62], L. Malentacca [47], A. Malinin [42], T. Maltsev [42], G. Manca [30,k], G. Mancinelli [12], C. Mancuso [28,13,o], R. Manera Escalero[44], D. Manuzzi [23], D. Marangotto [28,o], J.F. Marchand [10], R. Marchevski [48], U. Marconi [23], S. Mariani [47], C. Marin Benito [44], J. Marks [20], A.M. Marshall [53], G. Martelli [32,r], G. Martellotti [34], L. Martinazzoli [47], M. Martinelli [29,p], D. Martinez Santos [45], F. Martinez Vidal [46], A. Massafferri [2], R. Matev [47], A. Mathad [47], V. Matiunin [42], C. Matteuzzi [67], K.R. Mattioli [14], A. Mauri [60], E. Maurice [14], J. Mauricio [44], P. Mayencourt [48], J. Mazorra de Cos [46], M. Mazurek [40], M. McCann [60], L. Mcconnell [21], T.H. McGrath [61], N.T. McHugh [58], A. McNab [61], R. McNulty [21], B. Meadows [64], G. Meier [18], D. Melnychuk [40], F. M. Meng [4], M. Merk [36,76], A. Merli [48], L. Meyer Garcia [65], D. Miao [5,7], H. Miao [7], M. Mikhasenko [17,f], D.A. Milanes [73], A. Minotti [29,p], E. Minucci [67], T. Miralles [11], B. Mitreska [18], D.S. Mitzel [18], A. Modak [56], A. Mödden [18], R.A. Mohammed [62], R.D. Moise [16], S. Mokhnenko [42], T. Mombächer [47], M. Monk [55,1], S. Monteil [11], A. Morcillo Gomez [45], G. Morello [26], M.J. Morello [33,s], M.P. Morgenthaler [20], A.B. Morris [47], A.G. Morris [12], R. Mountain [67], H. Mu [4], Z. M. Mu [6], E. Muhammad [55], F. Muheim [57], M. Mulder [75], K. Müller [49], F. Muñoz-Rojas [9], R. Murta [60], P. Naik [59], T. Nakada [48], R. Nandakumar [56], T. Nanut [47], I. Nasteva [3], M. Needham [57], N. Neri [28,o], S. Neubert [17], N. Neufeld [47], P. Neustroev[42], J. Nicolini [18,13], D. Nicotra [76], E.M. Niel [48], N. Nikitin [42], P. Nogarolli [3], P. Nogga[17], N.S. Nolte [63], C. Normand [53], J. Novoa Fernandez [45], G. Nowak [64], C. Nunez [80], H. N. Nur [58],

A. Oblakowska-Mucha [38], V. Obraztsov [42], T. Oeser [16], S. Okamura [24,l], A. Okhotnikov [42],
O. Okhrimenko [51], R. Oldeman [30,k], F. Oliva [57], M. Olocco [18], C.J.G. Onderwater [76],
R.H. O'Neil [57], J.M. Otalora Goicochea [3], P. Owen [49], A. Oyanguren [46], O. Ozcelik [57], A.
Padee [40], K.O. Padeken [17], B. Pagare [55], P.R. Pais [20], T. Pajero [47], A. Palano [22],
M. Palutan [26], G. Panshin [42], L. Paolucci [55], A. Papanestis [56], M. Pappagallo [22,h],
L.L. Pappalardo [24,l], C. Pappenheimer [64], C. Parkes [61], B. Passalacqua [24], G. Passaleva [25],
D. Passaro [33,s], A. Pastore [22], M. Patel [60], J. Patoc [62], C. Patrignani [23,j], A. Paul [67],
C.J. Pawley [76], A. Pellegrino [36], J. Peng [5,7], M. Pepe Altarelli [26], S. Perazzini [23],
D. Pereima [42], H. Pereira Da Costa [66], A. Pereiro Castro [45], P. Perret [11], A. Perro [47],
K. Petridis [53], A. Petrolini [27,n], J. P. Pfaller [64], H. Pham [67], L. Pica [33,s], M. Piccini [32],
B. Pietrzyk [10], G. Pietrzyk [13], D. Pinci [34], F. Pisani [47], M. Pizzichemi [29,p], V. Placinta [41],
M. Plo Casasus [45], T. Poeschl [47], F. Polci [15,47], M. Poli Lener [26], A. Poluektov [12],
N. Polukhina [42], I. Polyakov [47], E. Polycarpo [3], S. Ponce [47], D. Popov [7], S. Poslavskii [42],
K. Prasanth [57], C. Prouve [45], V. Pugatch [51], G. Punzi [33,t], S. Qasim [49], Q. Q. Qian [6],
W. Qian [7], N. Qin [4], S. Qu [4], R. Quagliani [47], R.I. Rabadan Trejo [55], J.H. Rademacker [53],
M. Rama [33], M. Ramírez García [80], V. Ramos De Oliveira [68], M. Ramos Pernas [55],
M.S. Rangel [3], F. Ratnikov [42], G. Raven [37], M. Rebollo De Miguel [46], F. Redi [28,i],
J. Reich [53], F. Reiss [61], Z. Ren [7], P.K. Resmi [62], R. Ribatti [48], G. R. Ricart [14,81],
D. Riccardi [33,s], S. Ricciardi [56], K. Richardson [63], M. Richardson-Slipper [57], K. Rinnert [59],
P. Robbe [13], G. Robertson [58], E. Rodrigues [59], E. Rodriguez Fernandez [45],
J.A. Rodriguez Lopez [73], E. Rodriguez Rodriguez [45], A. Rogovskiy [56], D.L. Rolf [47],
P. Roloff [47], V. Romanovskiy [42], M. Romero Lamas [45], A. Romero Vidal [45], G. Romolini [24],
F. Ronchetti [48], T. Rong [6], M. Rotondo [26], S. R. Roy [20], M.S. Rudolph [67], T. Ruf [47],
M. Ruiz Diaz [20], R.A. Ruiz Fernandez [45], J. Ruiz Vidal [79,aa], A. Ryzhikov [42], J. Ryzka [38], J.
J. Saavedra-Arias [9], J.J. Saborido Silva [45], R. Sadek [14], N. Sagidova [42], D. Sahoo [74],
N. Sahoo [52], B. Saitta [30,k], M. Salomoni [29,p,47], C. Sanchez Gras [36], I. Sanderswood [46],
R. Santacesaria [34], C. Santamarina Rios [45], M. Santimaria [26,47], L. Santoro [2],
E. Santovetti [35], A. Saputi [24,47], D. Saranin [42], A. S. Sarnatskiy [75], G. Sarpis [57], M. Sarpis [61],
C. Satriano [34,u], A. Satta [35], M. Saur [6], D. Savrina [42], H. Sazak [16],
L.G. Scantlebury Smead [62], A. Scarabotto [18], S. Schael [16], S. Scherl [59], M. Schiller [58],
H. Schindler [47], M. Schmelling [19], B. Schmidt [47], S. Schmitt [16], H. Schmitz [17], O. Schneider [48],
A. Schopper [47], N. Schulte [18], S. Schulte [48], M.H. Schune [13], R. Schwemmer [47],
G. Schwering [16], B. Sciascia [26], A. Sciuccati [47], S. Sellam [45], A. Semennikov [42], T. Senger [49],
M. Senghi Soares [37], A. Sergi [27], N. Serra [49], L. Sestini [31], A. Seuthe [18], Y. Shang [6],
D.M. Shangase [80], M. Shapkin [42], R. S. Sharma [67], I. Shchemerov [42], L. Shchutska [48],
T. Shears [59], L. Shekhtman [42], Z. Shen [6], S. Sheng [5,7], V. Shevchenko [42], B. Shi [7], Q. Shi [7],
Y. Shimizu [13], E. Shmanin [42], R. Shorkin [42], J.D. Shupperd [67], R. Silva Coutinho [67],
G. Simi [31,q], S. Simone [22,h], N. Skidmore [55], T. Skwarnicki [67], M.W. Slater [52],
J.C. Smallwood [62], E. Smith [63], K. Smith [66], M. Smith [60], A. Snoch [36], L. Soares Lavra [57],
M.D. Sokoloff [64], F.J.P. Soler [58], A. Solomin [42,53], A. Solovev [42], I. Solovyev [42], R. Song [1],
Y. Song [48], Y. Song [4], Y. S. Song [6], F.L. Souza De Almeida [67], B. Souza De Paula [3],
E. Spadaro Norella [27], E. Spedicato [23], J.G. Speer [18], E. Spiridenkov [42], P. Spradlin [58],
V. Sriskaran [47], F. Stagni [47], M. Stahl [47], S. Stahl [47], S. Stanislaus [62], E.N. Stein [47],

O. Steinkamp [49], O. Stenyakin [42], H. Stevens [18], D. Strekalina [42], Y. Su [7], F. Suljik [62], J. Sun [30], L. Sun [72], Y. Sun [65], D. S. Sundfeld Lima [2], W. Sutcliffe [49], P.N. Swallow [52], F. Swystun [54], A. Szabelski [40], T. Szumlak [38], Y. Tan [4], M.D. Tat [62], A. Terentev [42], F. Terzuoli [33,w,47], F. Teubert [47], E. Thomas [47], D.J.D. Thompson [52], H. Tilquin [60], V. Tisserand [11], S. T'Jampens [10], M. Tobin [5,47], L. Tomassetti [24,l], G. Tonani [28,o,47], X. Tong [6], D. Torres Machado [2], L. Toscano [18], D.Y. Tou [4], C. Trippl [43], G. Tuci [20], N. Tuning [36], L.H. Uecker [20], A. Ukleja [38], D.J. Unverzagt [20], E. Ursov [42], A. Usachov [37], A. Ustyuzhanin [42], U. Uwer [20], V. Vagnoni [23], G. Valenti [23], N. Valls Canudas [47], H. Van Hecke [66], E. van Herwijnen [60], C.B. Van Hulse [45,y], R. Van Laak [48], M. van Veghel [36], G. Vasquez [49], R. Vazquez Gomez [44], P. Vazquez Regueiro [45], C. Vázquez Sierra [45], S. Vecchi [24], J.J. Velthuis [53], M. Veltri [25,x], A. Venkateswaran [48], M. Vesterinen [55], M. Vieites Diaz [47], X. Vilasis-Cardona [43], E. Vilella Figueras [59], A. Villa [23], P. Vincent [15], F.C. Volle [52], D. vom Bruch [12], N. Voropaev [42], K. Vos [76], G. Vouters [10,47], C. Vrahas [57], J. Wagner [18], J. Walsh [33], E.J. Walton [1,55], G. Wan [6], C. Wang [20], G. Wang [8], J. Wang [6], J. Wang [5], J. Wang [4], J. Wang [72], M. Wang [28], N. W. Wang [7], R. Wang [53], X. Wang[8], X. Wang [70], X. W. Wang [60], Y. Wang [6], Z. Wang [13], Z. Wang [4], Z. Wang [28], J.A. Ward [55,1], M. Waterlaat[47], N.K. Watson [52], D. Websdale [60], Y. Wei [6], J. Wendel [78], B.D.C. Westhenry [53], D.J. White [61], M. Whitehead [58], E. Whiter[52], A.R. Wiederhold [55], D. Wiedner [18], G. Wilkinson [62], M.K. Wilkinson [64], M. Williams [63], M.R.J. Williams [57], R. Williams [54], F.F. Wilson [56], W. Wislicki [40], M. Witek [39], L. Witola [20], C.P. Wong [66], G. Wormser [13], S.A. Wotton [54], H. Wu [67], J. Wu [8], Y. Wu [6], K. Wyllie [47], S. Xian[70], Z. Xiang [5], Y. Xie [8], A. Xu [33], J. Xu [7], L. Xu [4], L. Xu [4], M. Xu [55], Z. Xu [11], Z. Xu [7], Z. Xu [5], D. Yang [4], K. Yang [60], S. Yang [7], X. Yang [6], Y. Yang [27,n], Z. Yang [6], Z. Yang [65], V. Yeroshenko [13], H. Yeung [61], H. Yin [8], C. Y. Yu [6], J. Yu [69], X. Yuan [5], E. Zaffaroni [48], M. Zavertyaev [19], M. Zdybal [39], C. Zeng [5,7], M. Zeng [4], C. Zhang [6], D. Zhang [8], J. Zhang [7], L. Zhang [4], S. Zhang [69], S. Zhang [62], Y. Zhang [6], Y. Z. Zhang [4], Y. Zhao [20], A. Zharkova [42], A. Zhelezov [20], S. Z. Zheng [6], X. Z. Zheng [4], Y. Zheng [7], T. Zhou [6], X. Zhou [8], Y. Zhou [7], V. Zhovkovska [55], L. Z. Zhu [7], X. Zhu [4], X. Zhu [8], V. Zhukov [16], J. Zhuo [46], Q. Zou [5,7], D. Zuliani [31,q], G. Zunica [48]

[1] *School of Physics and Astronomy, Monash University, Melbourne, Australia*

[2] *Centro Brasileiro de Pesquisas Físicas (CBPF), Rio de Janeiro, Brazil*

[3] *Universidade Federal do Rio de Janeiro (UFRJ), Rio de Janeiro, Brazil*

[4] *Center for High Energy Physics, Tsinghua University, Beijing, China*

[5] *Institute Of High Energy Physics (IHEP), Beijing, China*

[6] *School of Physics State Key Laboratory of Nuclear Physics and Technology, Peking University, Beijing, China*

[7] *University of Chinese Academy of Sciences, Beijing, China*

[8] *Institute of Particle Physics, Central China Normal University, Wuhan, Hubei, China*

[9] *Consejo Nacional de Rectores (CONARE), San Jose, Costa Rica*

[10] *Université Savoie Mont Blanc, CNRS, IN2P3-LAPP, Annecy, France*

[11] *Université Clermont Auvergne, CNRS/IN2P3, LPC, Clermont-Ferrand, France*

[12] *Aix Marseille Univ, CNRS/IN2P3, CPPM, Marseille, France*

[13] *Université Paris-Saclay, CNRS/IN2P3, IJCLab, Orsay, France*

[14] *Laboratoire Leprince-Ringuet, CNRS/IN2P3, Ecole Polytechnique, Institut Polytechnique de Paris, Palaiseau, France*

[15] *LPNHE, Sorbonne Université, Paris Diderot Sorbonne Paris Cité, CNRS/IN2P3, Paris, France*

[16] *I. Physikalisches Institut, RWTH Aachen University, Aachen, Germany*

[17] *Universität Bonn — Helmholtz-Institut für Strahlen und Kernphysik, Bonn, Germany*

[18] *Fakultät Physik, Technische Universität Dortmund, Dortmund, Germany*

[19] *Max-Planck-Institut für Kernphysik (MPIK), Heidelberg, Germany*

[20] *Physikalisches Institut, Ruprecht-Karls-Universität Heidelberg, Heidelberg, Germany*

[21] *School of Physics, University College Dublin, Dublin, Ireland*

[22] *INFN Sezione di Bari, Bari, Italy*

[23] *INFN Sezione di Bologna, Bologna, Italy*

[24] *INFN Sezione di Ferrara, Ferrara, Italy*

[25] *INFN Sezione di Firenze, Firenze, Italy*

[26] *INFN Laboratori Nazionali di Frascati, Frascati, Italy*

[27] *INFN Sezione di Genova, Genova, Italy*

[28] *INFN Sezione di Milano, Milano, Italy*

[29] *INFN Sezione di Milano-Bicocca, Milano, Italy*

[30] *INFN Sezione di Cagliari, Monserrato, Italy*

[31] *INFN Sezione di Padova, Padova, Italy*

[32] *INFN Sezione di Perugia, Perugia, Italy*

[33] *INFN Sezione di Pisa, Pisa, Italy*

[34] *INFN Sezione di Roma La Sapienza, Roma, Italy*

[35] *INFN Sezione di Roma Tor Vergata, Roma, Italy*

[36] *Nikhef National Institute for Subatomic Physics, Amsterdam, Netherlands*

[37] *Nikhef National Institute for Subatomic Physics and VU University Amsterdam, Amsterdam, Netherlands*

[38] *AGH — University of Krakow, Faculty of Physics and Applied Computer Science, Kraków, Poland*

[39] *Henryk Niewodniczanski Institute of Nuclear Physics Polish Academy of Sciences, Kraków, Poland*

[40] *National Center for Nuclear Research (NCBJ), Warsaw, Poland*

[41] *Horia Hulubei National Institute of Physics and Nuclear Engineering, Bucharest-Magurele, Romania*

[42] *Affiliated with an institute covered by a cooperation agreement with CERN*

[43] *DS4DS, La Salle, Universitat Ramon Llull, Barcelona, Spain*

[44] *ICCUB, Universitat de Barcelona, Barcelona, Spain*

[45] *Instituto Galego de Física de Altas Enerxías (IGFAE), Universidade de Santiago de Compostela, Santiago de Compostela, Spain*

[46] *Instituto de Fisica Corpuscular, Centro Mixto Universidad de Valencia — CSIC, Valencia, Spain*

[47] *European Organization for Nuclear Research (CERN), Geneva, Switzerland*

[48] *Institute of Physics, Ecole Polytechnique Fédérale de Lausanne (EPFL), Lausanne, Switzerland*

[49] *Physik-Institut, Universität Zürich, Zürich, Switzerland*

[50] *NSC Kharkiv Institute of Physics and Technology (NSC KIPT), Kharkiv, Ukraine*

[51] *Institute for Nuclear Research of the National Academy of Sciences (KINR), Kyiv, Ukraine*

[52] *University of Birmingham, Birmingham, United Kingdom*

[53] *H.H. Wills Physics Laboratory, University of Bristol, Bristol, United Kingdom*

[54] *Cavendish Laboratory, University of Cambridge, Cambridge, United Kingdom*

[55] *Department of Physics, University of Warwick, Coventry, United Kingdom*

[56] *STFC Rutherford Appleton Laboratory, Didcot, United Kingdom*

[57] *School of Physics and Astronomy, University of Edinburgh, Edinburgh, United Kingdom*

[58] *School of Physics and Astronomy, University of Glasgow, Glasgow, United Kingdom*

[59] *Oliver Lodge Laboratory, University of Liverpool, Liverpool, United Kingdom*

[60] *Imperial College London, London, United Kingdom*

[61] *Department of Physics and Astronomy, University of Manchester, Manchester, United Kingdom*

[62] *Department of Physics, University of Oxford, Oxford, United Kingdom*

[63] *Massachusetts Institute of Technology, Cambridge, MA, United States*

[64] *University of Cincinnati, Cincinnati, OH, United States*

[65] *University of Maryland, College Park, MD, United States*

[66] *Los Alamos National Laboratory (LANL), Los Alamos, NM, United States*

[67] *Syracuse University, Syracuse, NY, United States*

[68] *Pontifícia Universidade Católica do Rio de Janeiro (PUC-Rio), Rio de Janeiro, Brazil, associated to* [3]

[69] *School of Physics and Electronics, Hunan University, Changsha City, China, associated to* [8]

[70] *Guangdong Provincial Key Laboratory of Nuclear Science, Guangdong-Hong Kong Joint Laboratory of Quantum Matter, Institute of Quantum Matter, South China Normal University, Guangzhou, China, associated to* [4]

[71] *Lanzhou University, Lanzhou, China, associated to* [5]

[72] *School of Physics and Technology, Wuhan University, Wuhan, China, associated to* [4]

[73] *Departamento de Fisica, Universidad Nacional de Colombia, Bogota, Colombia, associated to* [15]

[74] *Eotvos Lorand University, Budapest, Hungary, associated to* [47]

[75] *Van Swinderen Institute, University of Groningen, Groningen, Netherlands, associated to* [36]

[76] *Universiteit Maastricht, Maastricht, Netherlands, associated to* [36]

[77] *Tadeusz Kosciuszko Cracow University of Technology, Cracow, Poland, associated to* [39]

[78] *Universidade da Coruña, A Coruna, Spain, associated to* [43]

[79] *Department of Physics and Astronomy, Uppsala University, Uppsala, Sweden, associated to* [58]

[80] *University of Michigan, Ann Arbor, MI, United States, associated to* [67]

[81] *Departement de Physique Nucleaire (SPhN), Gif-Sur-Yvette, France*

[a] *Universidade de Brasília, Brasília, Brazil*

[b] *Centro Federal de Educacão Tecnológica Celso Suckow da Fonseca, Rio De Janeiro, Brazil*

[c] *Hangzhou Institute for Advanced Study, UCAS, Hangzhou, China*

[d] *School of Physics and Electronics, Henan University, Kaifeng, China*

[e] *LIP6, Sorbonne Universite, Paris, France*

[f] *Excellence Cluster ORIGINS, Munich, Germany*

[g] *Universidad Nacional Autónoma de Honduras, Tegucigalpa, Honduras*

[h] *Università di Bari, Bari, Italy*

[i] *Universita degli studi di Bergamo, Bergamo, Italy*

[j] *Università di Bologna, Bologna, Italy*

[k] *Università di Cagliari, Cagliari, Italy*

[l] *Università di Ferrara, Ferrara, Italy*

[m] *Università di Firenze, Firenze, Italy*

[n] *Università di Genova, Genova, Italy*

[o] *Università degli Studi di Milano, Milano, Italy*

[p] *Università degli Studi di Milano-Bicocca, Milano, Italy*

[q] *Università di Padova, Padova, Italy*

[r] *Università di Perugia, Perugia, Italy*

[s] *Scuola Normale Superiore, Pisa, Italy*

[t] *Università di Pisa, Pisa, Italy*

[u] *Università della Basilicata, Potenza, Italy*

[v] *Università di Roma Tor Vergata, Roma, Italy*

[w] *Università di Siena, Siena, Italy*

[x] *Università di Urbino, Urbino, Italy*

[y] *Universidad de Alcalá, Alcalá de Henares, Spain*

[z] *Facultad de Ciencias Fisicas, Madrid, Spain*

[aa] *Department of Physics/Division of Particle Physics, Lund, Sweden*

[†] *Deceased*